iScience

CellPress
OPEN ACCESS

Article

Islet cell stress induced by insulin-degrading enzyme deficiency promotes regeneration and protection from autoimmune diabetes

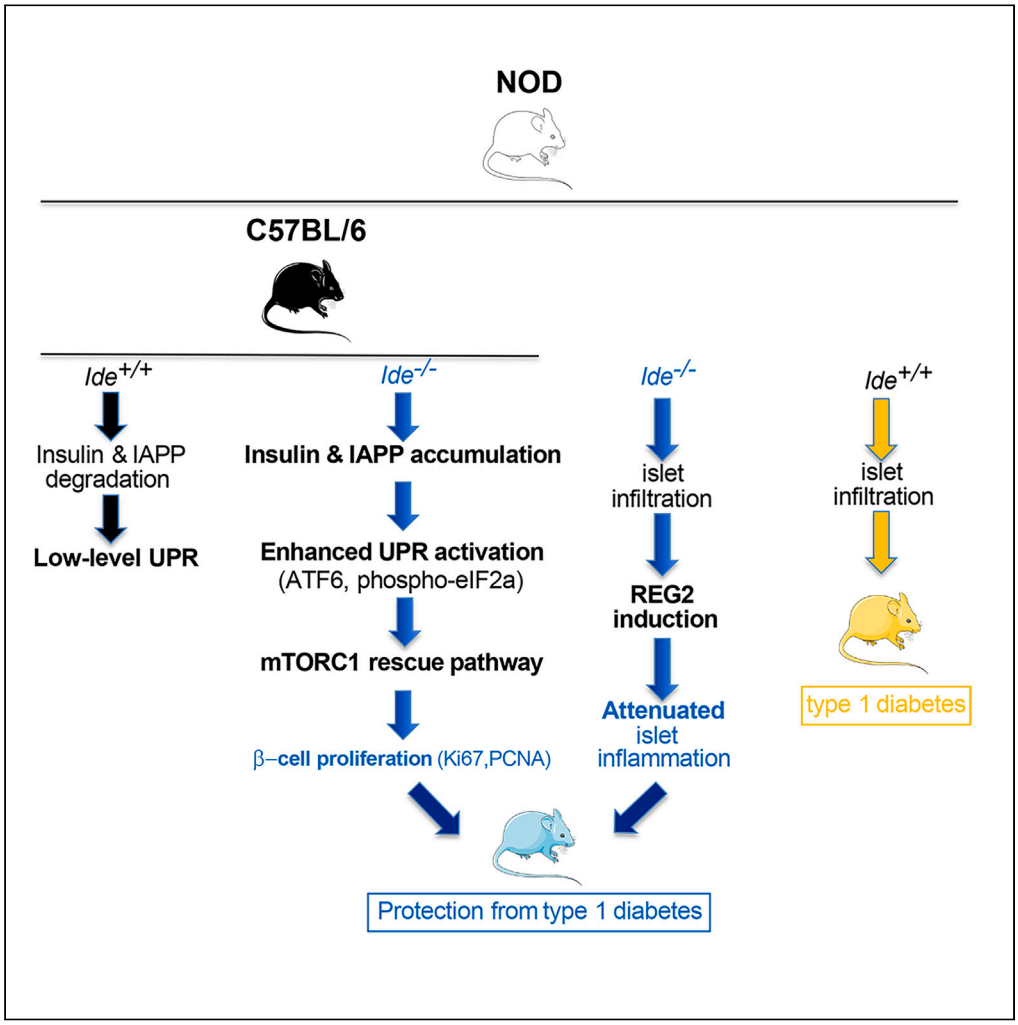

Shuaishuai Zhu, Emmanuelle Waeckel-Énée, Masaya Oshima, ..., Stefania Francesconi, François-Xavier Mauvais, Peter van Endert

vanendert@me.com

Highlights

Insulin-degrading enzyme (IDE) deficiency triggers an unfolded protein response

IDE deficiency results in beta cell proliferation dependent on mTORC1

IDE deficiency protects non-obese diabetic (NOD) mice from autoimmune diabetes

Autoimmune infiltration of IDE-deficient NOD islets triggers induction of REG2

Zhu et al., iScience 27, 109929
June 21, 2024
https://doi.org/10.1016/j.isci.2024.109929

iScience

CellPress
OPEN ACCESS

Article

Islet cell stress induced by insulin-degrading enzyme deficiency promotes regeneration and protection from autoimmune diabetes

Shuaishuai Zhu,[1,8] Emmanuelle Waeckel-Énée,[1] Masaya Oshima,[2] Anna Moser,[1] Marie-Andrée Bessard,[1] Abdelaziz Gdoura,[1] Kevin Roger,[3] Nina Mode,[2] Joanna Lipecka,[3] Ayse Yilmaz,[1] Barbara Bertocci,[1] Julien Diana,[1] Benjamin Saintpierre,[4] Ida Chiara Guerrera,[3] Raphael Scharfmann,[2] Stefania Francesconi,[5] François-Xavier Mauvais,[1,6] and Peter van Endert[1,7,9,*]

SUMMARY

Tuning of protein homeostasis through mobilization of the unfolded protein response (UPR) is key to the capacity of pancreatic beta cells to cope with variable demand for insulin. Here, we asked how insulin-degrading enzyme (IDE) affects beta cell adaptation to metabolic and immune stress. C57BL/6 and autoimmune non-obese diabetic (NOD) mice lacking IDE were exposed to proteotoxic, metabolic, and immune stress. IDE deficiency induced a low-level UPR with islet hypertrophy at the steady state, rapamycin-sensitive beta cell proliferation enhanced by proteotoxic stress, and beta cell decompensation upon high-fat feeding. IDE deficiency also enhanced the UPR triggered by proteotoxic stress in human EndoC-βH1 cells. In *Ide*$^{-/-}$ NOD mice, islet inflammation specifically induced regenerating islet-derived protein 2, a protein attenuating autoimmune inflammation. These findings establish a role of IDE in islet cell protein homeostasis, demonstrate how its absence induces metabolic decompensation despite beta cell proliferation, and UPR-independent islet regeneration in the presence of inflammation.

INTRODUCTION

Diabetes is the consequence of the failure of pancreatic beta cells to provide sufficient insulin to maintain normal blood glucose levels, due either to insulin resistance of tissue cells or to beta cell demise through an autoimmune response.[1] Physiologically, a sufficient insulin output is maintained by adaptive mechanisms including upregulation of beta cell secretory capacity but also beta cell proliferation and hyperplasia, together with protection from autoimmunity by regulatory T cells. Beta cell adaptation requires the mTORC1 (mammalian target of rapamycin 1) complex to activate and sustain protein translation, and the effectors of the UPR, a set of cellular pathways enabling the cell to cope with high protein loads in the endoplasmic reticulum (ER) by selective limitation of protein translation, increased production of chaperones, and upregulation of ER-associated protein degradation (ERAD).[2] While both mTORC1 and the UPR are critical for maintaining a beta cell mass adapted to metabolic needs, chronic and/or excessive activation of each of these interconnected pathways can result in beta cell failure and ultimately death[3]; for example, inhibiting mTORC1 by blocking eIF2a dephosphorylation with salubrinal promotes beta cell apoptosis.[4] However, the factors affecting the setpoints between beneficial and deleterious UPR and mTORC1 activation are not completely understood. Moreover, while it is now recognized that an efficient UPR contributes to beta cell resilience in the face of autoimmune aggression,[5] the interplay between beta cell physiology and autoimmunity remains insufficiently studied.

IDE is a ubiquitous endo-metalloprotease with high insulin affinity preferring small (≤10 kDa) substrates including some amyloidogenic peptides.[6–8] First identified as major insulin-degrading activity in hepatocytes, the role of IDE in physiologic insulin degradation remains unclear, given that mice with global or liver-restricted IDE deficiency display only mild hyperinsulinemia[9–11] and that endosomal insulin degradation by cathepsins has been described.[12] The wide expression in cells lacking insulin receptors as well as its high evolutionary conservation suggest that IDE may fulfill important functions beyond insulin degradation. Various lines of research have suggested a role of IDE in cellular

[1]Université Paris Cité, INSERM, CNRS, Institut Necker Enfants Malades, F-75015 Paris, France
[2]Université Paris Cité, CNRS, INSERM, Institut Cochin, F-75014 Paris, France
[3]Université Paris Cité, INSERM, CNRS, Structure Fédérative de Recherche Necker, Proteomics Platform, F-75015 Paris, France
[4]Université Paris Cité, INSERM, CNRS, Plateforme GENOM'IC, F-75015 Paris, France
[5]Genome Dynamics Unit, Institut Pasteur, Centre National de la Recherche Scientifique, UMR3525, F-75015 Paris, France
[6]Service de Physiologie – Explorations Fonctionnelles Pédiatriques, AP-HP, Hôpital Universitaire Robert Debré, F-75019 Paris, France
[7]Service Immunologie Biologique, AP-HP, Hôpital Universitaire Necker-Enfants Malades, F-75015 Paris, France
[8]Present address: Center for Reproductive Medicine, Department of Gynecology, Zhejiang Provincial People's Hospital, Affiliated People's Hospital, Hangzhou Medical College, Hangzhou, Zhejiang, China
[9]Lead contact
*Correspondence: vanendert@me.com
https://doi.org/10.1016/j.isci.2024.109929

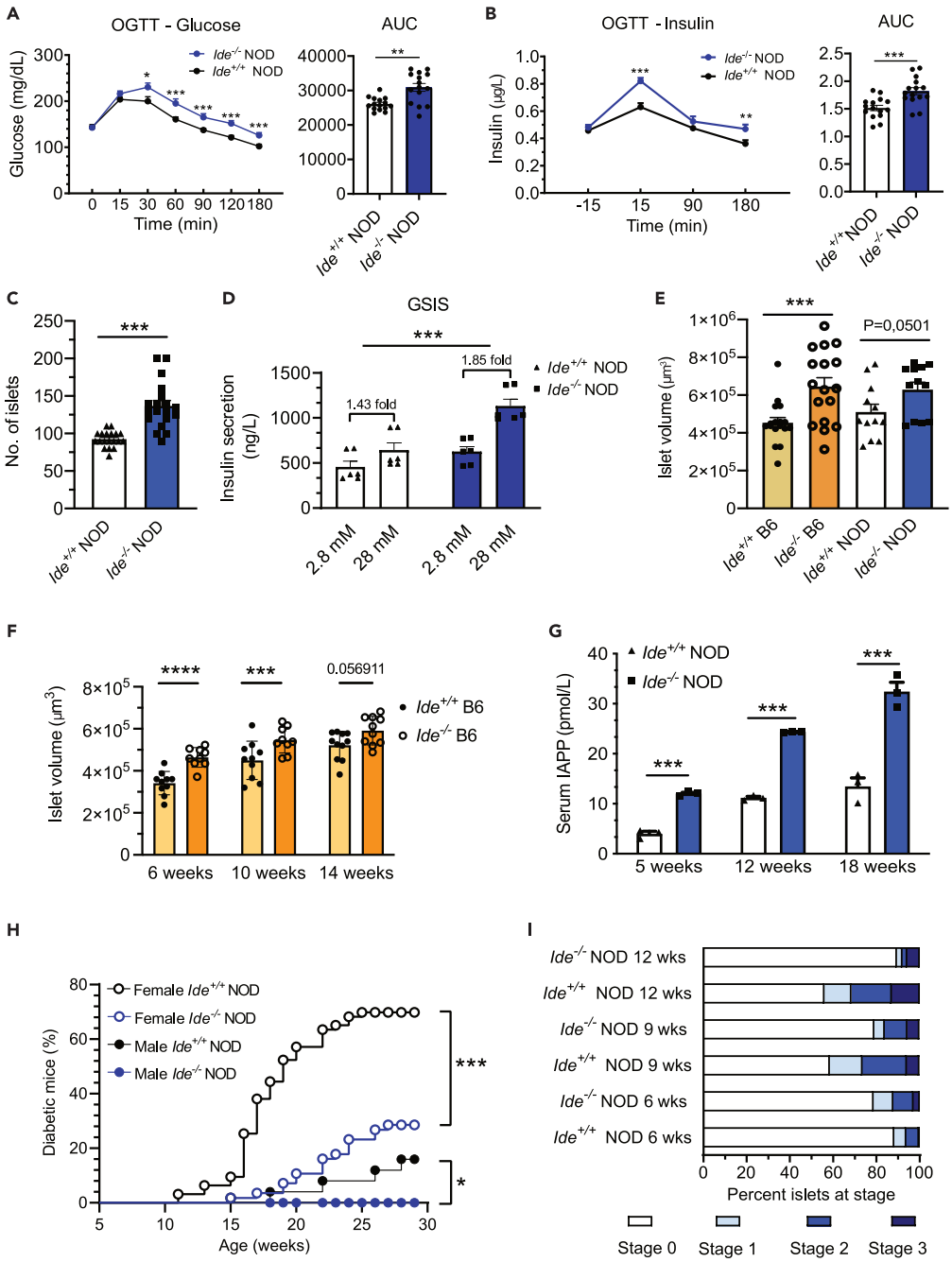

Figure 1. Beta cell function in *Ide*$^{-/-}$ C57BL/6J and NOD mice

(A) *Ide*$^{+/+}$ and *Ide*$^{-/-}$ NOD mice aged 14 weeks were subjected to an OGTT and glycemia was measured at indicated time points before (0 min) or after the glucose bolus. Data are mean values ±SEM of 15 independent mice for each group.

(B) Insulinemia during the OGTT as measured by ELISA. Data are mean values ±SEM of 15 independent mice for each group.

(C) Hand-picked islets obtained from female *Ide*$^{+/+}$ and *Ide*$^{-/-}$ NOD mice aged 8 weeks were counted in three separate experiments. Data are mean values ±SEM of 19 independent mice for each group.

(D) Following 90 min incubation without glucose, hand-picked islets from 10-week-old *Ide*$^{-/-}$ and *Ide*$^{+/+}$ NOD mice were sequentially incubated for 1 h in 2.8- and 28-mM glucose, and glucose-stimulated insulin secretion (GSIS) into the supernatant was quantified by commercial ELISA. Data are mean values ±SEM of 6 mice for each group.

(E) The volume of hand-picked islets from female C57BL/6 and NOD mice aged 8 weeks was calculated with Icy Software. Data are mean values ±SEM of an average of 15 mice for each group. Data in **A-E** were evaluated by Student's *t* test, *$p < 0.05$, **$p < 0.01$, ***$p < 0.001$.

(F) As in E but assessing the volume of islets of C57BL/6 *Ide*$^{+/+}$ and *Ide*$^{-/-}$ mice of different age. *N* = 8 per group.

Figure 1. *Continued*

(G) The amount of IAPP in the serum of female mice of different age was quantified by ELISA. Data are mean values ± SEM of 4 independent mice for each group. ***$p < 0.001$ by Student's *t* test.

(H) $Ide^{+/+}$ NOD and back-cross 10 $Ide^{-/-}$ NOD mice were monitored weekly for glycosuria until 29 weeks of age. Data are mean values ± SEM. $N = 63$ for female $Ide^{+/+}$, 57 for female $Ide^{-/-}$, 24 for male $Ide^{+/+}$, 29 for male $Ide^{-/-}$ mice. ***$p < 0.001$ by Kaplan-Meier, log rank (Mantel-Cox) test.

(I) Islets of pre-diabetic female $Ide^{+/+}$ and $Ide^{-/-}$ mice of different age were stained with hematoxylin/eosin and scored for insulitis. Score 0, no infiltration; 1, peri-insulitis; 2, moderate intra-insulitis (<50% of islet surface); 3, severe insulitis (>50 of surface and/or loss of islet architecture). Between 190 and 350 islets were counted for each group.

protein homeostasis. IDE interacts both with proteasome complexes and ubiquitin,[13,14] with a putative bimodal effect on proteasome activity.[15] IDE, which is induced by heat shock, has also been proposed to act as "dead-end chaperone",[16,17] for example forming complexes with aggregation-prone alpha-synuclein oligomers in beta cells[17] and with unfolded viral protein precursors,[18] or degrading beta amyloid in a parallel ERAD pathway.[19] Moreover, knockout of a fission yeast IDE homologue increases resistance to tunicamycin, a drug inducing a strong UPR, in a TORC1-dependent manner, suggesting a role in cellular stress responses.[20] *Ide* polymorphism is associated with fasting glucose levels and the risk of human type 2 diabetes.[21] Global, liver- and beta cell-restricted IDE deficiencies in C57BL/6 mice induce pronounced to mild glucose intolerance.[9–11,22] Conflicting results were obtained with inhibitors of the IDE active or regulatory sites, ranging from ameliorated to acutely compromised glucose tolerance.[23,24] Thus, IDE expression both in beta and liver cells moderately affects glucose metabolism, but how its role can be manipulated to ameliorate it remains unclear.

Prompted by evidence for a role of IDE in protein homeostasis, here, we studied C57BL/6 mice as well as NOD mice spontaneously developing autoimmune diabetes for activation of the UPR, inflammation, beta cell proliferation and glucose metabolism at the steady state and under metabolic, auto-immune or proteotoxic stress. We find that IDE deficiency protects NOD mice from autoimmune diabetes. Mechanistic studies reveal induction of a low-level UPR in both mouse strains associated with rapamycin-sensitive islet and beta cell proliferation but also metabolic decompensation upon high-fat feeding. In addition, our findings suggest that auto-immune infiltration of $Ide^{-/-}$ NOD islets specifically induces strong upregulation of REG2 (regenerating islet-derived protein 2), a protein known to attenuate inflammation and promoting proliferation, and potentially contributing to reduced expression of some inflammatory cytokines and protection from diabetes.

RESULTS

IDE-deficient NOD mice display beta cell hyperplasia/hypertrophy and dysfunction combined with protection from autoimmune diabetes

To produce $Ide^{-/-}$ NOD mice, we back-crossed previously published $Ide^{-/-}$ C57BL/6 mice[9] to NOD mice (Figure S1). $Ide^{-/-}$ NOD mice had normal fasting glucose and insulin levels (Figure 1A, B). In oral glucose tolerance tests (OGTT), $Ide^{-/-}$ NOD mice displayed slightly increased glycemia at several time points, associated with hyperinsulinemia, consistent with the findings of Farris and our previous findings.[24] Normoglycemic female $Ide^{-/-}$ NOD mice had significantly increased numbers of islets relative to WT mice (Figure 1C) which secreted higher amounts of insulin upon glucose stimulation *in vitro* (Figure 1D). Moreover, islets from 8-week-old $Ide^{-/-}$ mice had a larger volume, although the difference to WT islets reached significance only for C57BL/6 and not for NOD mice (Figure 1E). In C57BL/6 mice, islet hypertrophy due to IDE deficiency was most pronounced at 6 weeks of age and decreased gradually to lower levels at 10 and 14 weeks of age (Figure 1F).

Serum levels of islet amyloid polypeptide (IAPP), a well-known IDE substrate that is co-secreted with insulin and reduces post-prandial peaks of glycemia,[25,26] were strongly increased in $Ide^{-/-}$ NOD mice aged 5–18 weeks (Figure 1G), presumably due to the absence of IAPP degradation by IDE. Collectively, these results are consistent with a role of IDE in regulating insulin and IAPP levels in beta cells and suggest that young $Ide^{-/-}$ mice harbor an increased islet and beta cell mass which may result from beta cell hyperplasia, hypertrophy and/or regeneration, combined with compromised glucose tolerance and glucose-induced hyper-insulinemia.

Wondering how this beta cell dysfunction might affect manifestation of autoimmune diabetes, we monitored glycemia in $Ide^{-/-}$ NOD mice. IDE deficiency provided significant though incomplete protection from T1D to mice of both sexes, with 28% of $Ide^{-/-}$ vs. 70% of $Ide^{+/+}$ female ($p < 0.0001$), and 0% of $Ide^{-/-}$ vs. 17% of $Ide^{+/+}$ male ($p < 0.05$) animals manifesting hyperglycemia by 30 weeks (Figure 1H). This was associated with a decrease in islet inflammation between 6 and 12 weeks of age, contrasting with the well-known progressive increase in insulitis (stage 2 or 3) in $Ide^{+/+}$ NOD mice (Figure 1I).

IDE deficiency induces distinct stress responses in NOD and C57BL/6 pancreatic islets and in human beta cells

Although T2D eventually results in a reduced beta cell mass, an increased beta cell and insulin mass can develop to compensate for high metabolic demand in obesity, insulin resistance or due to beta cell-intrinsic factors.[27–29] The UPR is constitutively upregulated in beta cells and can induce a compensatory upregulation of beta cell mass and function.[30,31] Given our finding of an increased islet cell mass in $Ide^{-/-}$ islets (Figure 1) and literature suggestions of an IDE role in protein homeostasis as a chaperone and regulator of the proteasome-ubiquitin system, we asked whether $Ide^{-/-}$ islets displayed evidence of UPR upregulation.

We first tested fresh handpicked islets from pre-diabetic NOD mice and control C57BL/6 mice for expression of genes representing the three branches of the UPR, spliced X-Box binding protein 1 (*Xbp1s*) (indicating inositol-requiring enzyme 1alpha (IRE1α) activation), activating transcription factor 6 (*Atf6*), an UPR effector protecting cells from chronic stress,[32] and C/EBP homologous protein (CHOP (encoded by *Ddit3*) a pro-apoptotic protein downstream of protein kinase RNA-like endoplasmic reticulum kinase (PERK)). We also included

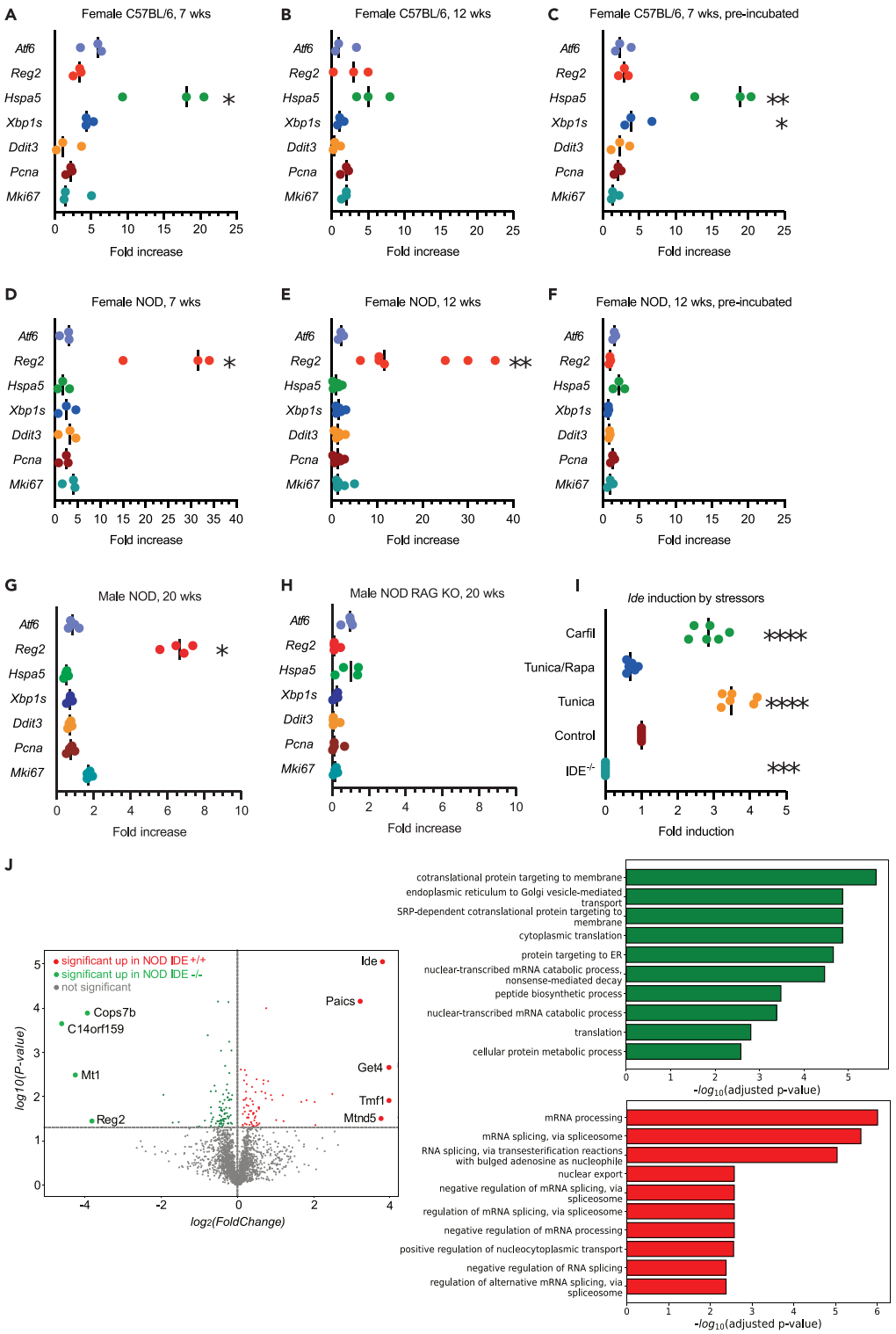

Figure 2. UPR effector mRNA and global protein expression by *Ide*$^{-/-}$ islet cells

(A–H) mRNA expression levels, as measured by RT-qPCR, of genes linked to the UPR (*Atf6*, *Hspa5*, *Xbp1s*, *Ddit3*), to regeneration (*Reg2*) or to proliferation (*Pcna*, *Mki67*) in steady state islets from *Ide*$^{+/+}$ and *Ide*$^{-/-}$ C57BL/6 and NOD mice of different ages, as indicated. Results are expressed as fold change, i.e., the ratio of expression in *Ide*$^{-/-}$ relative to *Ide*$^{+/+}$ islets. Islets were either analyzed immediately after isolation or after overnight culture in RPMI medium, as indicated. Each

Figure 2. *Continued*

dot represents islets from one mouse. Data in A–H were evaluated by Mann-Whitney tests with Bonferroni correction for multiple comparisons. $p < 0.05$, $^{**}p < 0.01$, $^{***}p < 0.001$, $^{****}p < 0.0001$.

(I) *Ide*$^{+/+}$ or control *Ide*$^{-/-}$ NOD mice aged 10 weeks were injected for 2 weeks with carfilzomib or for 2 days with tunicamycin with or without addition of rapamycin before isolation of islets and quantification of *Ide* mRNA expression by RT-qPCR. Data were evaluated by two-way ANOVA with Dunnett's multiple comparison correction. $^{***}p < 0.001$, $^{****}p < 0.0001$.

(J) Proteomic analysis of islet proteins from 3 *Ide*$^{+/+}$ and 3 *Ide*$^{-/-}$ mice aged 10 weeks. Left: volcano plot showing the proteins up- (in green) and down- (in red) regulated in *Ide*$^{-/-}$ NOD islets. The horizontal dashed line represents the significance threshold (*p*-value <0.05) (for details see Table S1). Right: Barplot representing the Gene Ontology Biological Process (GO BP) terms enriched using enrichR software and the GO Biological Process 2021 database. In green are the TOP10 GO BP terms enriched using the up-regulated proteins in *Ide*$^{-/-}$ and in red the TOP10 GO BP terms enriched using the up-regulated proteins in *Ide*$^{+/+}$ islets for analysis. A log-transformed adjusted *p*-value was used for TOP10 ranking (for details see Table S2).

immunoglobulin-binding protein (BIP; encoded by *Hspa5*), an ER chaperone with a key role in the UPR,[33] proliferating cell nuclear antigen (*Pcna*) and Ki67 (encoded by *Mki67*) as markers of proliferation, and regenerating islet-derived 2 (*Reg2*), encoding a protein expressed in regenerating islets but not at all in normal islets.[34,35] REG2 has been reported to increase the beta cell mass, ameliorate diabetes in NOD mice and attenuate the UPR and apoptosis.[36–38]

Islets from female *Ide*$^{-/-}$ C57BL/6 mice aged 7 weeks displayed strong upregulation of *Hspa5* mRNA but not of other UPR or proliferation markers; *Hspa5* upregulation became non-significant at 12 weeks. This upregulation was maintained after overnight culture of islets, suggesting that BIP induction was due to an islet-intrinsic mechanism (Figure 2A-C). In striking contrast, islets from *Ide*$^{-/-}$ female NOD mice aged 7 or 12 weeks lacked BIP induction but displayed strong *Reg2* upregulation (Figure 2D, E). However, this was completely lost upon overnight culture (Figure 2F), a procedure resulting in rapid exit of infiltrating immune cells from islets.[39] Therefore, upregulation of *Reg2* may be triggered by autoimmune infiltration. Supporting this conclusion, islets devoid of inflammation from *Ide*$^{-/-}$ *Rag2*$^{-/-}$ mice completely lacked *Reg2* induction, and islets from male *Ide*$^{-/-}$ mice with attenuated infiltration displayed lower *Reg2* induction that was also rapidly lost *ex vivo* (Figure 2G, H, Figure S2A, B). Taken together, these results suggested that the absence of IDE induces a mild UPR characterized by selective upregulation of *Hspa5* in C57BL/6 islets, consistent with perturbed cellular protein homeostasis in the absence of Ide. Conversely *Ide*$^{-/-}$ NOD islet cells upregulate a key marker of regeneration in the presence of inflammation but fail to upregulate *Hspa5*, possibly in relation to a defective UPR reported for this strain.[5]

Having observed evidence of perturbed protein homeostasis in islet and beta cells, we examined the ultrastructure of *Ide*$^{-/-}$ beta cells by electron microscopy (Figure S3A, B). This confirmed an increased average size of beta cells while the total area of dense core structures, i.e., insulin content appeared normal (Figure S3C, D). However, the appearance of mature secretory granules was dramatically altered in *Ide*$^{-/-}$ beta cells, with greatly enlarged halos potentially corresponding in part to fused and/or mixed organelles[40] (Figure S3B, E). Presumably because of the massive halo enlargement, beta cells contained a lower number of granules despite their increased average total area (Figure S3C, F). Thus, IDE deficiency greatly perturbs the appearance of beta cell granules however without apparent effect on their overall insulin content.

To obtain additional evidence for a role of IDE in islet cell protein homeostasis, we treated NOD mice for two days with a proteasome inhibitor or tunicamycin and examined *Ide* mRNA levels by islets. *Ide* expression was strongly upregulated by both drugs, consistent with a role in the response to proteotoxic stress (Figure 2I). Interestingly, mTORC1 inhibition by rapamycin abolished the effect of tunicamycin on *Ide* expression, suggesting that IDE levels may correlate with the global level of protein translation in stressed cells.

To obtain a broad view on the effect of IDE deficiency on islet protein expression, we subjected lysates of *Ide*$^{+/+}$ and *Ide*$^{-/-}$ NOD islets to a global proteomic analysis. Analysis of protein abundance revealed that both WT and *Ide*$^{-/-}$ cells were enriched for pathways related to mRNA processing (Figure 2J). Proteins in *Ide*$^{-/-}$ islets were also enriched for translation of ER-targeted proteins and ER to Golgi protein transport (Figure 2J and Tables S1 and S2), a finding that could be related to an upregulated UPR. Differentially expressed genes in WT cells included the BAG6/BAT3 complex (Get4), a platform for sorting of proteins between the ER and the ER-associated degradation (ERAD) pathway, and Tmf1 (TATA element modulatory factor), a protein essential for Glut4 trafficking to Glut4 storage vesicles. *Tmf*$^{-/-}$ mice develop hyperglycemia due to compromised glucose uptake.[41] Proteins upregulated in *Ide*$^{-/-}$ cells included the proteasome-associated COP9 signalosome (Cops7b), which decreases protein ubiquitylation by SCF-type E3 ligases, metallothionein (Mt1), involved in zinc ion homeostasis and upregulated in beta cell stress, and importantly REG2 (Figure 2J). This was not due to absence of REG2 degradation by IDE which was unable to digest REG2 even upon prolonged *in vitro* incubations (Figure S2C, D). Collectively these results are consistent with a role of IDE of protein homeostasis the perturbation of which can affect regulation of protein translation and degradation, as well as secretory pathway transport.

To obtain additional insight on the relationship between IDE expression and protein homeostasis, we next analyzed islets obtained from mice treated with tunicamycin which induces strong ER stress. Tunicamycin had little effect on expression of the genes tested in *Ide*$^{+/+}$ islets while it induced some markers of ER stress in *Ide*$^{-/-}$ cells, although this did not reach significance due to high variance (Figure S4A-C). In WT NOD islets, tunicamycin induced a moderate upregulation of *Xbp1s*, *Reg2* and *Ddit3* (Figure S4D). In contrast, *Ide*$^{-/-}$ NOD islets displayed induction of *Mki67* whereas *Reg2* was downregulated (Figure S4G). Thus, *Reg2* is upregulated by islet inflammation but downregulated by proteotoxic stress in *Ide*$^{-/-}$ NOD islets. The combination of tunicamycin with the mTOR inhibitor rapamycin induced *Xbp1s* both in *Ide*$^{+/+}$ and *Ide*$^{-/-}$ islets relative to untreated islets, combined with proliferation as indicated by *Pcna* or *Mki67* upregulation, respectively (Figure S4E, H). However, compared to islets exposed to tunicamycin only, rapamycin addition had little effect though it surprisingly stimulated *Mki67* expression by *Ide*$^{+/+}$ islets (Figure S4F, I).

To determine whether IDE is also involved in protein homeostasis in human beta cells, we next analyzed the effect of *IDE* knockdown in EndoC-βH1 cells, an immortalized human cell line expressing many features of beta cells including reversion of diabetes in mice.[42] siRNA knockdown decreased *IDE* expression by 80% in EndoC cells (Figure S5A). Incubation of EndoC cells with drugs inducing proteotoxic stress strongly upregulated *IDE* expression like in primary murine islets (Figure S5B, Figure 2I). Induction of proteotoxic stress in EndoC cells strongly induced *HSPA5*, *DDIT3* and both total and spliced *XBP1* (Figure S5C-F). *IDE* knockdown moderately increased upregulation of *HSPA5* upon epoxomicin exposure, and of *XBP1(S)* upon tunicamycin exposure (Figure S5C, F, F). These results are consistent with a role of IDE in protein homeostasis in human beta cells. We also could test the effect of pharmacological IDE inhibition in primary human islets. Incubation with BDM44768, a specific competitive IDE inhibitor,[24] induced strongly upregulation of *HSPA5* and moderate induction of *MKI67* expression (Figure S5G). Although the latter data is anecdotal, it is consistent with our observations for EndoC cells.

We also examined ER stress signaling at the protein level. At the steady state, PERK and eIF2α phosphorylation, ATF6 nuclear translocation and PCNA expression did not differ between WT and $Ide^{-/-}$ C57BL/6 mice (Figure 3A-G). Tunicamycin induced PERK phosphorylation, ATF6 cleavage and PCNA expression in $Ide^{-/-}$ islets, an effect abolished by mTORC1 inhibition, but had no significant effect on stress effector proteins in WT islets (Figure 3B-G). Thus, C57BL/6 $Ide^{-/-}$ islet cells display increased sensitivity to massive proteotoxic stress. In contrast to C57BL/6 islets, steady state islets from $Ide^{-/-}$ NOD mice aged 9–15 weeks were characterized by a partial stress response absent in WT islets, with phosphorylated eIF2α but not PERK, increased nuclear ATF6 and upregulated PCNA (Figure 3H-N). Thus, islets from $Ide^{-/-}$ NOD mice displayed a specific partial UPR next to REG2 mRNA induction which may be due to their genetic background and/or to the presence of autoimmune inflammation, the latter being consistent with the results shown in Figure 2G, H.

IDE deficiency modulates inflammatory signaling differentially in C57BL/6 versus NOD mice

Considering that ER stress and insulin signaling can induce an inflammatory response,[43] we next examined islets for expression of inflammatory marker mRNA. Steady state islets from young (aged 4 to 12 weeks) female $Ide^{-/-}$ NOD mice displayed downregulation of IL-1β (*Il1b*) mRNA and strong downregulation of 2′-5′-oligoadenylate synthase 3 (*Oas3*), a key enzyme in type 1 interferon signaling, up to the age of 12 weeks while *Oas3* was upregulated at 15 weeks; the latter could be related to ER stress in older NOD mice (Figure 3L, M). Expression of additional inflammatory genes was not altered (Figure 4, Figure S6A). mRNA expression of a subset of markers in male NOD islets was not altered (Figure S6B). After short-term tunicamycin treatment of female NOD mice, *Oas3* expression remained low while expression of some inflammatory markers (*Nlrp3*, *Mcp1*, *Ifil27a*) was moderately increased (Figure 4B).

Contrasting with NOD islets, expression of *Tnfa*, *Nlrp3* and *Il1b* mRNA was increased in steady state islets from $Ide^{-/-}$ C57BL/6 as compared to $Ide^{+/+}$ mice. Tunicamycin treatment strongly increased expression of these and *Il6* mRNA in $Ide^{+/+}$ and $Ide^{-/-}$ islets, with expression by $Ide^{-/-}$ islets remaining superior (Figure 4C). Thus, IDE deficiency had a markedly different effect on transcription of inflammatory effectors, with significant to strong activation in $Ide^{-/-}$ C57BL/6 islets contrasting with downregulation in young $Ide^{-/-}$ NOD islets.

High fat diet induces obesity and decompensation of glucose metabolism in $ide^{-/-}$ mice

Considering our observations of compromised glucose tolerance and islet hyperplasia in $Ide^{-/-}$ mice (Figure 1), we subjected WT and $Ide^{-/-}$ C57BL/6 mice to high fat diet (HFD) for 7 weeks and monitored glucose metabolism and ER stress markers. In $Ide^{-/-}$ mice, HFD resulted in a massive weight gain by almost 70%, contrasting with 30% in WT mice; $Ide^{-/-}$ mice on standard diet were not overweight (Figure 5A, B). This was accompanied by massive hyperinsulinemia and even stronger hyperproinsulinemia in $Ide^{-/-}$ mice fed HFD (Figure 5C, E). HFD increased the amount of insulin and proinsulin in WT islets about 6-fold and in $Ide^{-/-}$ mice 10-fold (Figure 5D, F); however, despite this massive upregulation of (pro-)insulin production, WT mice developed moderate and $Ide^{-/-}$ mice substantial hyperglycemia (Figure 5G).

Next, we examined the effect of metabolic stress on UPR and proliferation markers. Both in $Ide^{+/+}$ and $Ide^{-/-}$ mice, HFD induced ER stress as indicated by upregulation of *Hspa5* and *Xbp1s* together with the proliferation marker *Mki67* that was more pronounced in $Ide^{-/-}$ mice; *Reg2* expression was downregulated in mice of both genotypes (Figure 5H, I). However, contrasting with the induction of UPR markers by IDE deficiency in the absence of metabolic stress (Figure 5J), IDE deficiency had little effect in mice fed HFD (Figure 5K). Thus, the main effect of IDE deficiency in beta cells is a mild UPR induction in the absence of metabolic stress, potentially associated with an enhanced proliferative response in its presence.

Given the association of increased (pro-)insulin output by beta cells with UPR induction, we wondered whether conversely inducing a UPR can induce insulin output by islet cells. Indeed, tunicamycin treatment *in vivo* significantly induced islet accumulation and secretion of insulin in both $Ide^{+/+}$ and $Ide^{-/-}$ NOD mice (Figure S7A, C) while its effect on proinsulin accumulation and secretion did not reach significance (Figure S7B, D). This experiment also provided additional evidence for an increased insulin content in, and secretion by, $Ide^{-/-}$ islet cells (Figure S7A, C).

IDE deficiency induces beta cell proliferation enhanced by metabolic and pharmacologic stress

Beta cells adapt to high metabolic demand through ER expansion but also through proliferation.[3] We analyzed islets at the steady state and from mice exposed to metabolic or pharmacologic stress for expression of Ki67 and incorporation of 5-ethynyl-2′-deoxyuridine (EdU). At the steady state, NOD $Ide^{-/-}$ islets contained up to 6-fold more Ki67 spots than WT islets. Tunicamycin upregulated Ki67 expression strongly in both WT and $Ide^{-/-}$ NOD islets but more so in the latter, an effect abolished by rapamycin and by salubrinal, an inhibitor of eIF2α dephosphorylation (Figure 6A, B, C). Steady state $Ide^{-/-}$ C57BL/6 islets also displayed significantly higher Ki67 staining than WT islets, a difference amplified in mice fed an HFD (Figure 6D, E). Upregulation of proliferation i.e., Ki67 expression characterized not only total islet cells but also beta cells (Figure 6F). Finally, to directly measure DNA replication in steady state beta cells, we compared EdU incorporation in

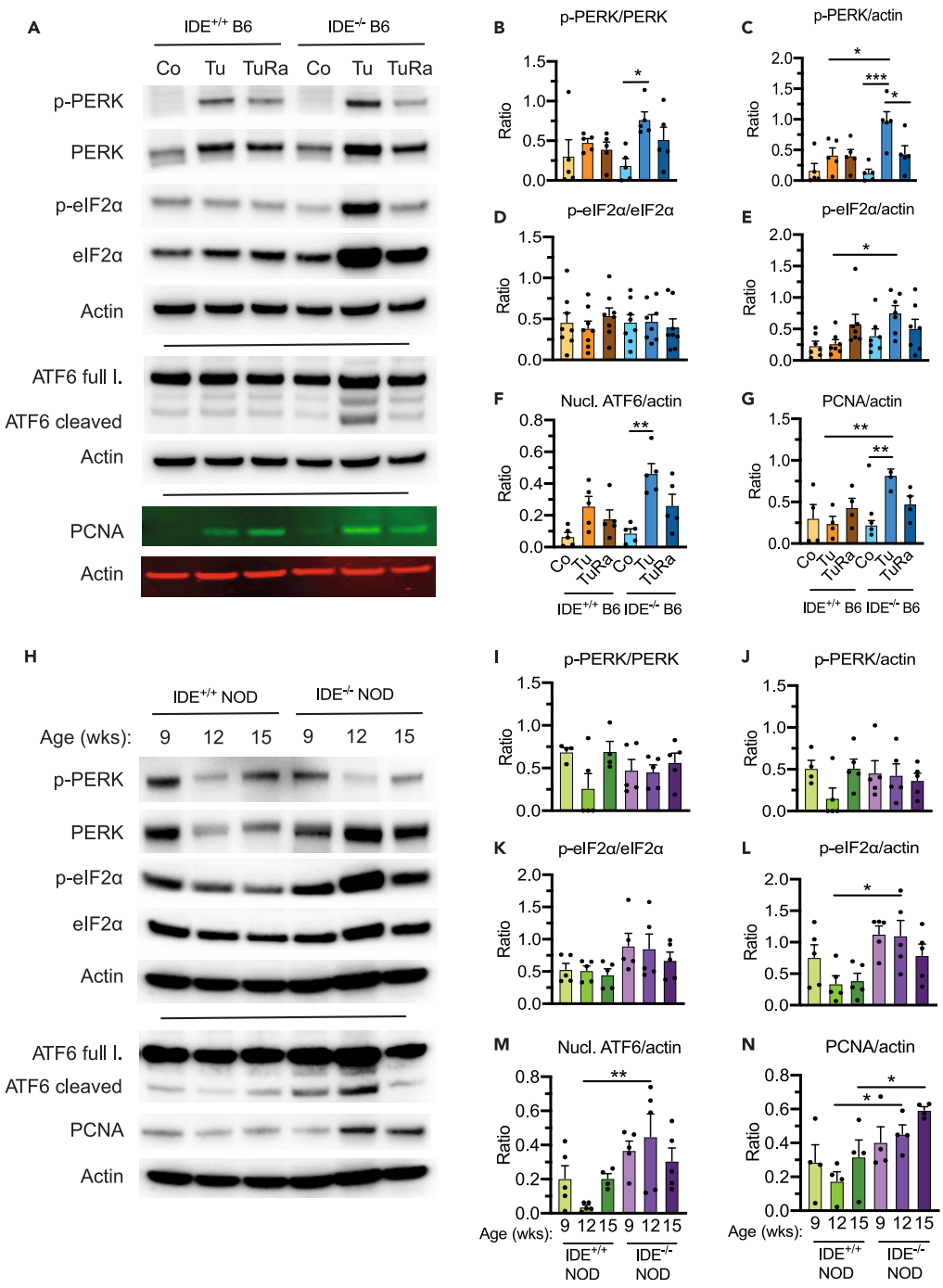

Figure 3. Immunoblot analysis of UPR effector activation

(A) Representative immunoblots showing the expression pattern of phosphorylated PERK, total PERK, phosphorylated eIF2α, total eIF2α, ATF6, cleaved ATF6, and PCNA in islet lysates of C57BL/6 *Ide*$^{+/+}$ and *Ide*$^{-/-}$ mice treated by tunicamycin injection i.p., combined with rapamycin or not, for 48 h.

(B–G) quantification of experiments performed as shown in (**A**), $N = 5$ in (**B**), 5 in (**C**), 8 in (**D**), 7 in (**E**), 5 in (**F**) and 4 in (**G**). Data represent the ratio of *Ide*$^{-/-}$ to *Ide*$^{+/+}$ islets, are represented as mean ± SEM and were evaluated by Student's *t* test in **B-F** and by ANOVA with Tukey's correction for multiple comparisons in (**G**). *$p < 0.05$, **$p < 0.02$.

(H) Representative protein immunoblots as in **A** but for steady state islets from *Ide*$^{+/+}$ and *Ide*$^{-/-}$ NOD mice aged 9, 12 or 15 weeks.

(I–N) quantification of experiments performed as shown in (**H**). $N = 5$ for panels **I-M** and 4 for **N**. Data are represented as mean ± SEM and were evaluated by Student's *t* test; *$p < 0.05$.

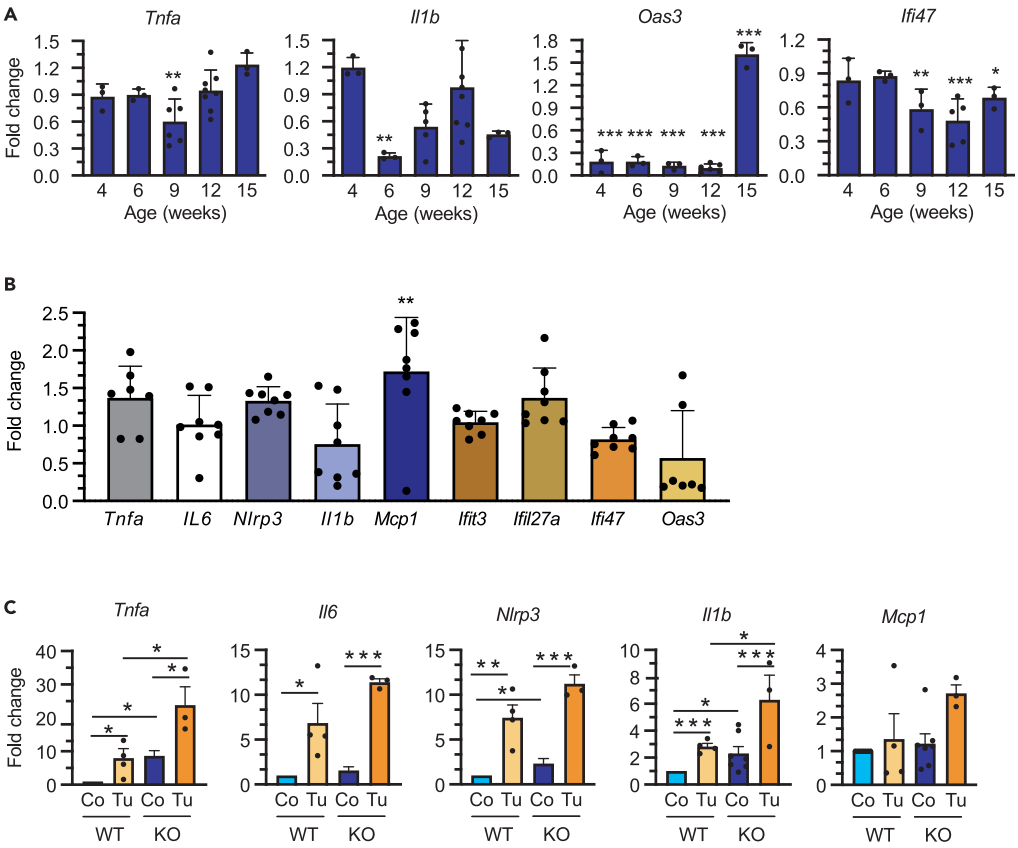

Figure 4. Effect of IDE deficiency on expression of inflammatory genes

(A) RT-qPCR analysis of relative *Tnfa*, *Il1b*, *Oas3*, and *Ifi47* expression in islets of female *Ide*$^{+/+}$ and *Ide*$^{-/-}$ NOD mice aged 4 to 15 weeks. Results represent the ratio of expression in *Ide* $^{-/-}$ relative to *Ide* $^{+/+}$ islets and are mean values ±SEM of 3–6 independent mice for each group. *$p < 0.05$, **$p < 0.02$, and ***$p < 0.01$ by Student's *t* test.

(B) mRNA expression of the indicated genes in the islets of *Ide*$^{-/-}$ relative to *Ide*$^{+/+}$ NOD mice treated with tunicamycin for 48 h. Data are mean values ±SEM of 8 independent mice for each group. *$p < 0.05$, **$p < 0.02$, and ***$p < 0.01$ by Student's *t* test for panels A and B.

(C) mRNA expression of the indicated genes in *Ide*$^{-/-}$ relative to *Ide*$^{+/+}$ islets from C57BL/6 mice aged 15 to 25 weeks treated with tunicamycin for 48 h. Data are mean values ±SEM of 6 independent mice for each group. *$p < 0.05$, **$p < 0.02$, and ***$p < 0.01$ by ANOVA test with Tukey's correction.

insulin-positive cells. EdU incorporation was increased at the steady state both in *Ide*$^{-/-}$ C57BL/6 and NOD beta cells (Figure 6G-I). Thus, *Ide*$^{-/-}$ islet and beta cells display substantial constitutive upregulation of proliferation that is further increased by metabolic stress. Proteotoxic stress enhances proliferation in WT and *Ide*$^{-/-}$ cells in a manner dependent on mTORC1 activation and on eIF2α dephosphorylation.

RNA-seq analysis confirms upregulation of *ide*$^{-/-}$ islet cell proliferation upon HFD

To obtain initial mechanistic insight in the response of islet cells to ER stress, we performed RNA-seq analysis on C57BL/6 mice subjected to HFD for 2 weeks. Gene expression among islets from 3 *Ide*$^{-/-}$ and 5 *Ide*$^{+/+}$ mice correlated and *Ide*$^{-/-}$ islets clustered in principle component analysis while expression by WT mice was more heterogeneous (Figure S8A, B). Top genes enriched in *Ide*$^{-/-}$ islets were related to cycling, including *lockd* (long non-coding RNA regulating Cdkn1b), *Ckap2* (cytoskeleton-associated protein 2); and to stress responses: *Pyroxd2* (Pyridine-nucleotide disulfide oxidoreductase) and *Gsto2* (glutathione S-transferase omega-2) (Figure S8C). Gene set enrichment analysis of differentially expressed genes indicated strong enrichment of cellular processes related to cell cycle, mitosis, cytokinesis and mRNA processing in *Ide*$^{-/-}$ islets from HFD-fed mice (Figure S8E); all five top gene sets were related to mitosis and cell cycle (Figure 7A). In contrast, genes differentially expressed in *Ide*$^{+/+}$ islets were strongly enriched in metabolic pathways related to amino acid metabolism and peptide chain elongation (Figure 7B; Figure S8E).

Analysis of differentially expressed genes did not reveal strong enrichment of stress response pathways (Figure S8D). Examination of individual genes involved in the IRE1 and PERK-mediated UPR and the integrated stress response revealed absence of upregulation or even downregulation of key genes such as *Ern* (encoding IRE1), *Eif2ak3* (encoding PERK) but also *Hspa5* in *Ide*$^{-/-}$ islets (Figure 7C). Interestingly, two key genes ensuring a high level of translation during stress responses by inhibiting eIF2α phosphorylation, *Impact* and *Qrich1*, were significantly upregulated in the absence of *Ide* expression (Figure 7C).[44,45] Thus, while IDE deficiency induces a moderate UPR at the steady state, it

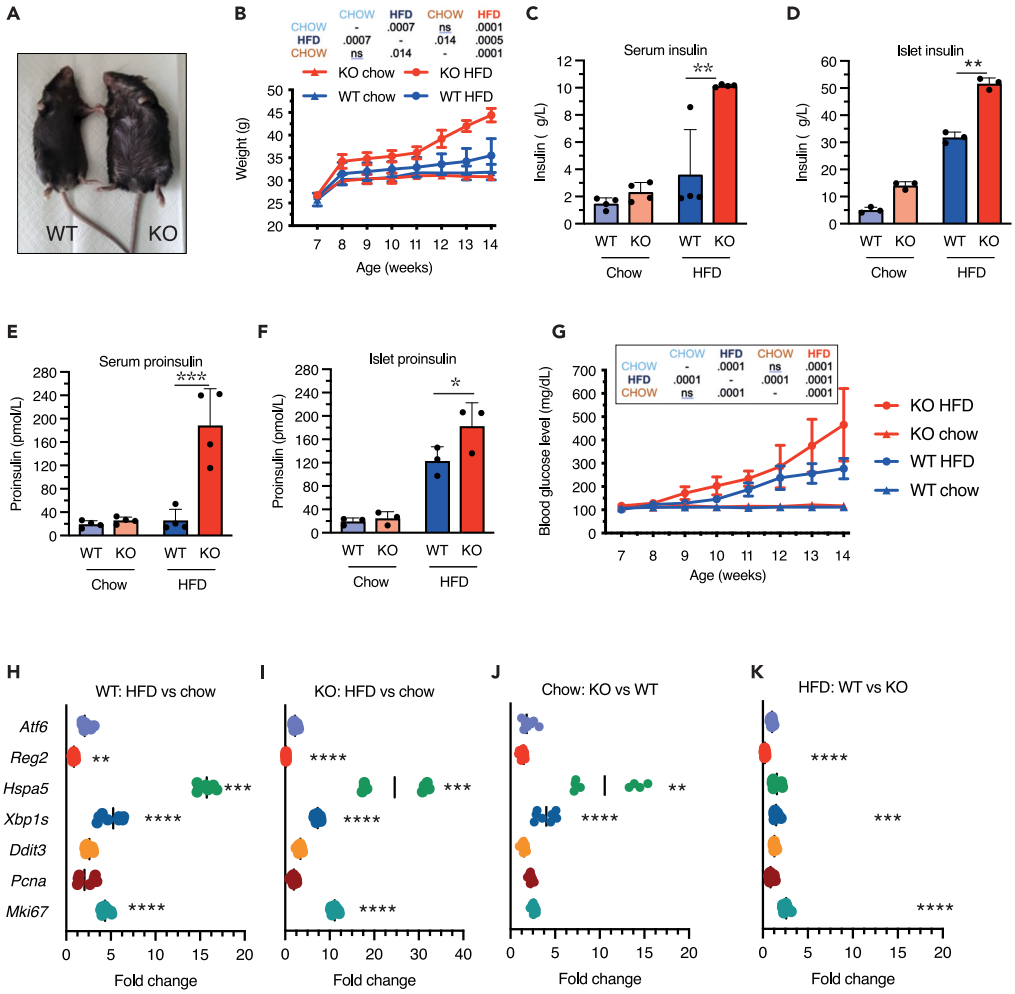

Figure 5. Effect of IDE deficiency on the metabolic and UPR response to HFD

Seven-week-old female *Ide*$^{-/-}$ and *Ide*$^{+/+}$ C57BL/6J mice were fed a standard chow or HFD for 7 weeks. *N* = 10 per group.

(A) Representative appearance of *Ide*$^{+/+}$ and *Ide*$^{-/-}$ mice at sacrifice.

(B) Body weight was recorded once a week. Data are mean values ±SEM. Statistical significance is indicated in the insert.

(C–F) Serum insulin and proinsulin levels and total insulin and proinsulin content in islets were determined for *Ide*$^{-/-}$ and *Ide*$^{+/+}$ mice at the time of sacrifice, N = 3–4 per group.

(G) Non-fasting glucose concentrations were monitored weekly; *N* = 8 per group.

(H–K) Expression levels of genes related to ER stress, proliferation, and regeneration, as measured by RT-qPCR, in islets obtained at sacrifice of *Ide*$^{-/-}$ and *Ide*$^{+/+}$ mice fed standard chow or HFD, *N* = 8. Results are expressed as ratio of expression as indicated: **H**, HFD vs. standard chow for *Ide*$^{+/+}$ mice; **I**, HFD vs. standard chow for *Ide*$^{-/-}$ mice; **J**, *Ide*$^{-/-}$ vs. *Ide*$^{+/+}$ for standard chow-fed; **K**, *Ide*$^{-/-}$ vs. *Ide*$^{+/+}$ for HFD-fed mice. All panels show mean values ±SEM, plus individual data points in **H–K**. Statistical evaluation was performed by two-way ANOVA with Dunnett's or Dunn's correction for multiple comparisons. *$p < 0.05$, **$p < 0.01$, ***$p < 0.001$, ****$p < 0.0001$.

may promote maintained protein translation upon metabolic stress, thereby enhancing proliferation, without increasing islet cell stress in this situation.

Considering the link between UPR and inflammation and the enrichment in GO terms related to the immune system process (Figure S8D), we also analyzed immune-related gene sets. WT islets were enriched in genes related to antigen uptake (lectins, FcγR, C1q), antigen presentation (H-2Eβ) and processing (*Cd74* and *Ctss*; encoding invariant chain and cathepsin S) (Figure 7D). Collectively, these data confirmed strong upregulation of proliferation in metabolically stressed C57BL/6 *Ide*$^{-/-}$ islets and suggested that IDE deficiency may reduce immune activation in this condition.

DISCUSSION

In the context of islet cell biology, IDE has previously been studied essentially with respect to its role in glucose metabolism and insulin degradation. While we confirm previous findings such as compromised glucose tolerance and increased insulin content in *Ide*$^{-/-}$ islets, we have

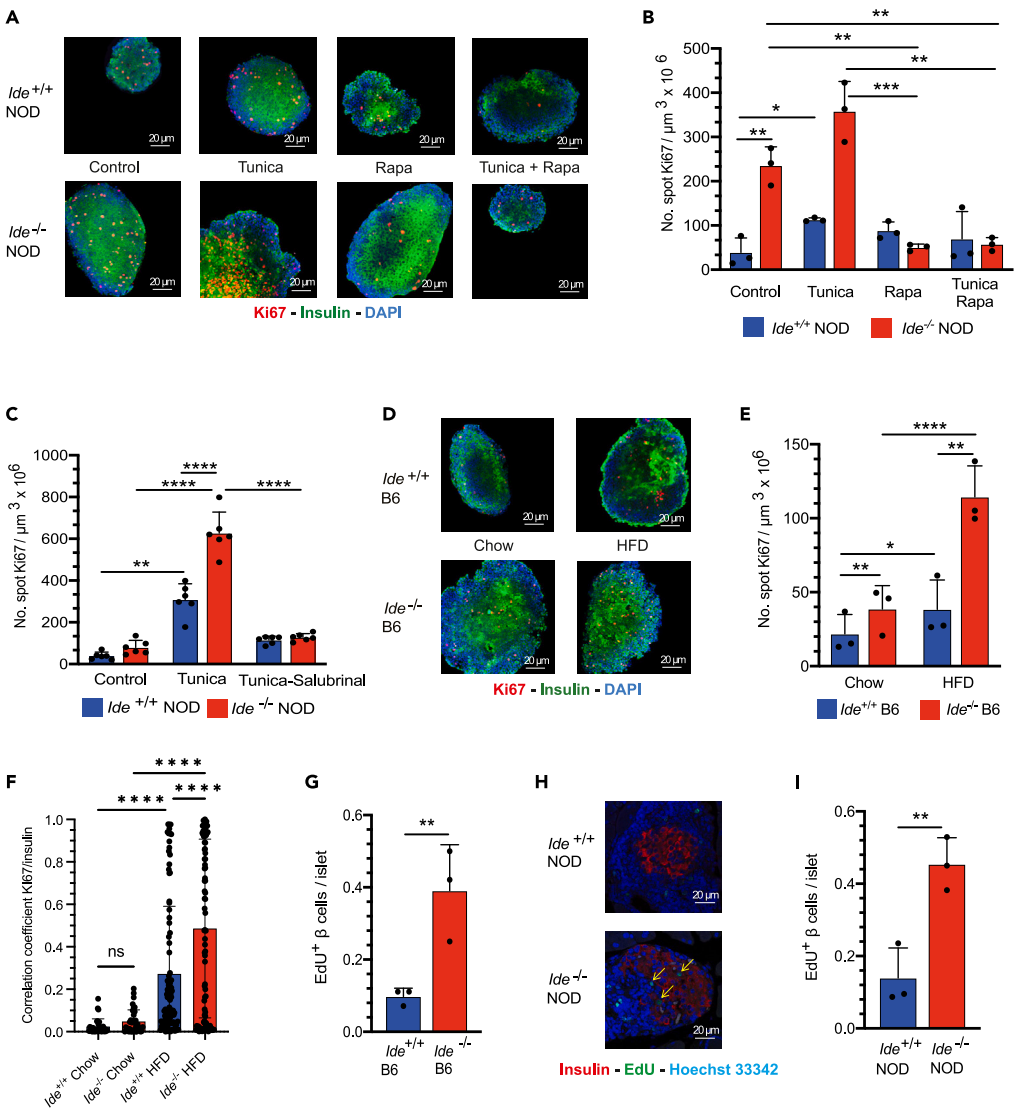

Figure 6. Effect of proteotoxic or metabolic stress and of IDE deficiency on islet cell proliferation

(A) Representative images stained for insulin (green) and Ki67 (red) of islets of female *Ide*$^{-/-}$ or *Ide*$^{+/+}$ NOD mice aged 12 weeks and treated for 2 days with tunicamycin and/or rapamycin or solvent alone.

(B) Number of Ki67 spots per volume for the conditions indicated in (**A**). *N* = 3 per group, with an average of 40 islets per mouse counted.

(C) *Ide*$^{-/-}$ and *Ide*$^{+/+}$ NOD mice aged 12 weeks were treated for 2 days as in (**A**), however using tunicamycin alone or combined with salubrinal. Quantitative evaluation as in (**B**). *N* = 6 per group.

(D) Representative images, stained for insulin and Ki67, showing islets from *Ide*$^{-/-}$ and *Ide*$^{+/+}$ C57BL/6 mice aged 14 weeks, after an HFD or standard diet for 7 weeks.

(E) Quantitative evaluation as in (**B**) of the experiment shown in (**D**). *N* = 3 per group.

(F) Female 7-week-old *Ide*$^{+/+}$ and *Ide*$^{-/-}$ C57BL/6 mice were kept on a high-fat diet or standard chow for 8 weeks. Then the coefficient of proximity between insulin and Ki67 staining was calculated for 20 planes of 15 islets for each group. Statistical evaluation by Student's *t* test.

(G) EdU incorporation in insulin stained cells of *Ide*$^{-/-}$ and *Ide*$^{+/+}$ C57BL/6 mice after treatment with tunicamycin for 2 days followed by administration of EdU for 1 h was quantified. *N* = 3 mice per group, with on average 55 islets per mouse evaluated.

(H) Representative immunofluorescence images showing insulin expression and EdU incorporation in steady state islets from *Ide*$^{-/-}$ and *Ide*$^{+/+}$ NOD mice aged 12 weeks. The arrows point to EdU^{+} beta cells.

(I) Quantification of EdU^{+} beta cells in (**H**). *N* = 3 mice per group, with on average 66 islets per mouse counted. The numbers of Ki67^{+} spots in panels **B, C, E** and the numbers of EdU^{+} beta cells in **G, I** are represented as mean ± SEM. Statistical analysis was performed for panels B, C, E and G by two-way ANOVA with Sidak's correction for multiple comparisons and for panel I by unpaired t-test. *$p < 0.05$, **$p < 0.01$, ***$p < 0.001$, ****$p < 0.0001$.

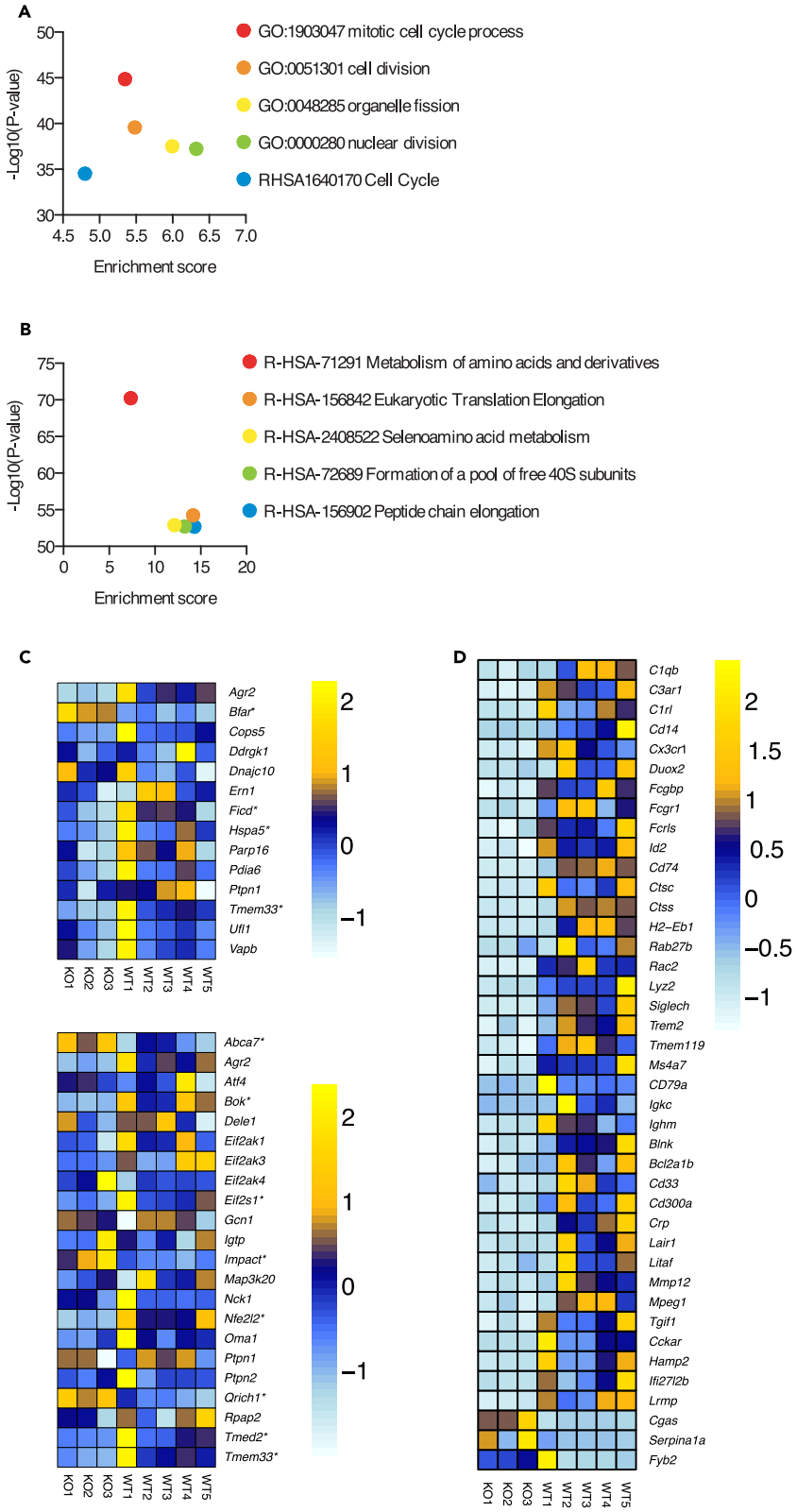
A
-Log10(P-value)
Enrichment score
GO:1903047 mitotic cell cycle process
GO:0051301 cell division
GO:0048285 organelle fission
GO:0000280 nuclear division
RHSA1640170 Cell Cycle
B
-Log10(P-value)
Enrichment score
R-HSA-71291 Metabolism of amino acids and derivatives
R-HSA-156842 Eukaryotic Translation Elongation
R-HSA-2408522 Selenoamino acid metabolism
R-HSA-72689 Formation of a pool of free 40S subunits
R-HSA-156902 Peptide chain elongation
C
Agr2
Bfar*
Cops5
Ddrgk1
Dnajc10
Ern1
Ficd*
Hspa5*
Parp16
Pdia6
Ptpn1
Tmem33*
Ufl1
Vapb
Abca7*
Agr2
Atf4
Bok*
Dele1
Eif2ak1
Eif2ak3
Eif2ak4
Eif2s1*
Gcn1
Igtp
Impact*
Map3k20
Nck1
Nfe2l2*
Oma1
Ptpn1
Ptpn2
Qrich1*
Rpap2
Tmed2*
Tmem33*
KO1 KO2 KO3 WT1 WT2 WT3 WT4 WT5
D
C1qb
C3ar1
C1rl
Cd14
Cx3cr1
Duox2
Fcgbp
Fcgr1
Fcrls
Id2
Cd74
Ctsc
Ctss
H2–Eb1
Rab27b
Rac2
Lyz2
Siglech
Trem2
Tmem119
Ms4a7
CD79a
Igkc
Ighm
Blnk
Bcl2a1b
Cd33
Cd300a
Crp
Lair1
Litaf
Mmp12
Mpeg1
Tgif1
Cckar
Hamp2
Ifi27l2b
Lrmp
Cgas
Serpina1a
Fyb2
KO1 KO2 KO3 WT1 WT2 WT3 WT4 WT5

Figure 7. Expression of selected genes in *Ide*$^{+/+}$ and *Ide*$^{-/-}$ islets of mice subjected to metabolic stress

(A and B) Enriched pathways were calculated and clustered by adjusted *p*-values by automatic Metascape algorithm. Dot plots show the adjusted –Log$_{10}$(*p*-value) and Enrichment score for the top 5 pathways specifically enriched in *Ide*$^{-/-}$ **A** and *Ide*$^{+/+}$ **B** samples.

(C) Color heatmap (*Z* score) of genes from GO:0036498:IRE1-mediated unfolded protein response (top), and GO:0036499: PERK-mediated unfolded protein response and GO:140467:integrated stress response signaling (bottom). The asterisk * marks differentially expressed genes between *Ide*$^{-/-}$ and *Ide*$^{+/+}$ samples with an adjusted *p*-value <0.05.

(D) Color heatmap (*Z* score) of key genes selected from the list of differentially expressed genes (adjusted *p*-value<0.01, l2fc > 2) and classified into general into immune system. See also Figure S6.

uncovered a role of IDE in protein homeostasis of murine and human islet and beta cells revealed by a basal activation of the UPR in unstressed cells and mTORC1-dependent proliferation both in the presence and absence of metabolic or proteotoxic stress. We show that the role of IDE in protein homeostasis extends to human islet and beta cells that display an enhanced UPR and strong upregulation of IDE upon proteotoxic stress as well as induction of *HSPA5* and *MKI67* upon IDE inhibition. We also reveal a clearly distinct response to IDE deficiency in immune cell-infiltrated NOD islets associated with an attenuated inflammatory response, possibly related to the induction of *Reg2* expression. Thus, both at the steady state and upon massive proteotoxic stress, IDE deficiency provides the unexpected benefits of inducing C57BL/6 and NOD islet cell proliferation dependent on mTORC1 activity but not on REG2, whereas production of the anti-inflammatory molecule REG2 is induced only in inflamed NOD islets and abolished by massive proteotoxic stress.

Although not previously described, a role of IDE in islet protein homeostasis is consistent, next to its high affinity for insulin, with evidence for interaction with, and regulation of, the ubiquitin-proteasome system, and its direct induction by proteotoxic stress (Figure 2I). Increased insulin and IAPP content of *Ide*$^{-/-}$ islets suggests a key role of IDE in degrading these substrates in beta cells. The effect of tunicamycin treatment on accumulation of these substrates likely is indirect, as folding of neither of these substrates is affected by inhibition of N-glycosylation. IDE can form non-proteolytic complexes with other substrates, e.g., alpha-synuclein[17] or a VZV protein precursor.[46]

At the steady state, IDE deficiency induced a mild UPR with hallmark activation of ATF6 and eIF2α phosphorylation in the absence of PERK activation (Figure 3I-M). Proteotoxic stress can activate other kinases of the integrated stress response phosphorylating eIF2α; for example, proteasome dysfunction is sensed by protein kinase R.[47] As IDE may be involved in cytosolic recycling of amino acids from low molecular weight proteins, its absence might also be sensed by general control non-derepressible-2 kinase (GCN2).[48] Relative enrichment of pathways related to amino acid metabolism in WT islets from HFD-fed mice (Figure 7) would be consistent with such a scenario.

Our results suggest a modest upregulation of the UPR in *Ide*$^{-/-}$ cells, limited to *Hspa5* mRNA upregulation in C57/BL6 islets and increased ATF6 cleavage in NOD islets at the steady state. In *Ide*$^{-/-}$ C57BL/6 islets, both islet hypertrophy and Hspa5 induction are strongest in young mice, suggesting a causal relationship. A low-level UPR or HFD feeding has been observed by multiple authors to be sufficient for induction of beta cell proliferation,[3,49,50] with an important role of ATF6.[51,52] In line with these reports, we document enhanced proliferation of *Ide*$^{-/-}$ islet and beta cells, further amplified by proteotoxic or metabolic stress. Enhanced proliferation also characterizes *Ide*$^{-/-}$ pancreatic alpha cells[53]; although the exact mechanism remains unclear, Merino et al. suggested a link with reduced cilia formation, or a role of IDE interaction with PTEN.[54] Hyperplasia of, and excessive hormone output by, pancreatic endocrine cells upon conditional or global IDE deletion may indicate an important functional role of IDE in secretory processes that remains to be deciphered.[22,53]

Tunicamycin-triggered proliferation depended on mTORC1 activity and was inhibited by salubrinal, suggesting a requirement for reversing stress-induced eIF2α phosphorylation. In stress situations, mTORC1 can orchestrate an anabolic rescue program, activating amino acid transport and protein synthesis via ATF4 activation[55]; prolonged activation of this program can result in beta cell apoptosis. Elevated serum levels and islet content of proinsulin, observed in HFD-fed *Ide*$^{-/-}$ mice, are a hallmark of beta cell dysfunction and suggest unabated mTORC1 activation. Taken together these findings suggest that stressed *Ide*$^{-/-}$ beta cells may upregulate an mTORC1-dependent rescue pathway, enhancing proliferation at low but inducing beta cell dysfunction at high metabolic stress levels.

The massive weight gain of *Ide*$^{-/-}$ C57BL/6 mice exposed to an HFD suggests that unabated mTORC1 activation may extend beyond islet cells, aided or driven by high insulin output of beta cells. The ubiquitous expression and evolutionary conservation of IDE are well-known arguments for an organism-wide important role of IDE in metabolism, but such a role remains largely enigmatic.[8] This concerns even the complex role of IDE in glucose metabolism, which is impacted by IDE degradation of insulin and glucagon.[23] Confusingly, mice lacking IDE exclusively in the liver display glucose intolerance and insulin resistance although plasma insulin levels are normal.[11] An organism-wide role of IDE may also be related to its role in regulating the ubiquitin-proteasome system, as "dead-end chaperone", or affecting autophagy.[7,10,15]

Such an enigmatic organism-wide role notwithstanding, our findings on the ultrastructure of *Ide*$^{-/-}$ beta cells suggest a strong perturbation of insulin granule biology. The appearance of insulin granules in *Ide*$^{-/-}$ beta cells is closely reminiscent of beta cells lacking *Atp6ap2*, an accessory component of the vacuolar V-ATPase.[56] Very similar to *Atp6ap2*$^{-/-}$ beta cells, we observed large multigranular vacuoles. The authors of that paper speculated that Atp6ap2 could restrain secretory granule fusion upstream of the induction of autophagy. Whether IDE regulates secretory granule trafficking and processing, potentially linked to V-ATPase components, remains to be determined.

Potentially the most interesting result was the strong upregulation of *Reg2* mRNA and protein exclusively in infiltrated *Ide*$^{-/-}$ islets from NOD mice. REG2 is secreted by beta cells and may act in an autocrine fashion.[34] Treatment of NOD mice with REG2 may reduce the incidence of autoimmune diabetes and increase the beta cell area.[37] In tunicamycin-treated MIN6 insulinoma cells, over-expression of REG2 attenuated Ire1α and PERK in response to tunicamycin while upregulating BIP and at the same time phosphorylation of mTORC1 and of its substrate S6K1.[38] Thus, the literature links REG2 to an attenuated UPR, reduced inflammation and mTORC1 activation. Although we have no genetic proof for a causal relationship, in our hands, REG2 upregulation is associated with reduced levels of inflammatory cytokines in young NOD

mice, and at the steady state with evidence of mTORC1 activation. However, REG2 is not required for proliferation and in fact downregulated in the presence of proteotoxic and metabolic islet cell stress. Attenuated inflammation, an ameliorated UPR and a mTORC1-driven regeneration/proliferation program may contribute to protection from autoimmune diabetes.

We are aware that proteolytic processing of insulin, the key autoantigen in the NOD model of autoimmune diabetes,[57] by IDE may affect disease and have studied T cell responses to insulin in *Ide*$^{-/-}$ mice; these studies indicate that altered presentation of insulin peptides by beta cells also contributes to protection from disease (manuscript in preparation). In any case, beta cell regeneration and an attenuated UPR have both and independently been shown to protect NOD mice from autoimmune diabetes,[5,51] rendering a contribution of the present findings in *Ide*$^{-/-}$ islet cells to protection plausible.

How could the protective effect of IDE deficiency in NOD mice link to the genetic association of *IDE* with type 2 diabetes? Efforts to develop inhibitors for therapeutic use in this condition[23,58] also assume a detrimental role of IDE, although this is based on direct inhibition of hormone degradation which may not be the main function of IDE as discussed above. If we assume instead that IDE plays an important but ill-defined role in protein homeostasis and regulation of secretion in endocrine cells, many scenarios protecting from both type 1 and type 2 diabetes can be envisaged. For example, an efficient moderately activated UPR inducing proliferation will be beneficial in both conditions.

The beneficial effect of IDE deficiency on beta cell proliferation and autoimmune inflammation raises the question of the interest of therapeutic IDE inhibition. IDE inhibitors have previously been proposed to be of interest to ameliorate glucose metabolism in type 2 diabetes patients, and more recently also to reduce autoimmune inflammation in the NOD model. Maianti et al. found that an inhibitor competing with substrate binding ameliorated glucose tolerance in an OGTT,[23] while we found that administration of an active site inhibitor compromised glucose tolerance in the same test.[24] The reason for this discrepancy remains unclear. A novel inhibitor designed by Nash et al. binding to the central substrate binding cavity reportedly provides protection from diabetes in NOD mice, seemingly consistent with our data[58]; *Reg2* expression was not studied by these authors. However, in contrast to our results, this inhibitor improves rather than compromises glucose tolerance in HFD-mice and does not induce weight gain, therefore, probably does not trigger mTORC1 activation. Collectively, these findings indicate that our mechanistic understanding of the effects of IDE inhibition remains poor. Our finding that IDE deficiency activates not only proliferation but also an anti-inflammatory pathway indicates that biological effects of IDE unrelated to insulin degradation remain of significant interest for future research.

Limitations of the study

Although our data suggest strongly that IDE deficiency modulates (pro-)insulin homeostasis in beta cells, it remains to be determined how exactly IDE regulates (pro-)insulin and IAPP levels in beta cells, and how this triggers a mild UPR. The potential role of IDE in secretory granule trafficking or processing also remains to be elucidated. Moreover, how IDE deficiency induces REG2 upregulation in NOD islets selectively in the presence of autoimmune inflammation will be an important question for future studies.

STAR★METHODS

Detailed methods are provided in the online version of this paper and include the following:

- KEY RESOURCES TABLE
- RESOURCE AVAILABILITY
  - Lead contact
  - Materials availability
  - Data and code availability
- EXPERIMENTAL MODEL AND STUDY PARTICIPANT DETAILS
  - Animals
- METHOD DETAILS
  - Insulitis scoring
  - Spontaneous diabetes incidence
  - Oral glucose tolerance test (OGTT)
  - Estimation of islet volume
  - Pancreatic islet preparation
  - IAPP quantification in serum
  - Glucose-stimulated insulin secretion (GSIS)
  - RNA preparation and qPCR analysis
  - Digestions with recombinant IDE
  - Electron microscopy
  - Proteomic analysis of NOD islets
  - ER stress
  - EndoC-βH1 experiments
  - Primary human islet test
  - Immunoblots

- HFD treatment and follow up
- Immunocytology
- EdU staining
- RNAseq analysis

- QUANTIFICATION AND STATISTICAL ANALYSIS

SUPPLEMENTAL INFORMATION

Supplemental information can be found online at https://doi.org/10.1016/j.isci.2024.109929.

ACKNOWLEDGMENTS

This work was supported by a grant from the European Foundation for the Study of Diabetes (EFSD/Lilly Program 2017), grant ANR-18-CE92-0008-01 from the Agence Nationale de la Recherche, and grant EQU201903007853 from the Fondation pour la Recherche Médicale to PvE. Work performed in the laboratory of RS was supported by the Dutch Diabetes Research Foundation and the DON Foundation. We are grateful to A. Schmitt (Electronic Microscopy Facility, INSERM UMR1016, Cochin Institute, Paris, France) for electron microscopy analysis, to Rebecca Deprez-Poulain (Institut Pasteur de Lille) for the inhibitor BDM44768, and to Vinson Liang and Wei-Jen Tang, University of Chicago, who provided recombinant IDE enzyme, with support through grant NIH R01 GM121964.

AUTHOR CONTRIBUTIONS

S.Z. and E.W.E.: investigation, visualization; M.A., A.M., M.A.B., A.G., J.L., K.R., N.M., A.Y., and B.B.: investigation; B.S.P., C.I.G., and F.X.M.: formal analysis; J.D. and S.F.: conceptualization; R.S.: funding acquisition; P.V.E.: conceptualization, funding acquisition, administration, supervision, visualization, writing, editing.

DECLARATION OF INTERESTS

The authors declare no competing interests.

Received: October 25, 2023
Revised: March 8, 2024
Accepted: May 3, 2024
Published: May 7, 2024

REFERENCES

1. Roden, M., and Shulman, G.I. (2019). The integrative biology of type 2 diabetes. Nature *576*, 51–60. https://doi.org/10.1038/s41586-019-1797-8.
2. Wang, J., Yang, X., and Zhang, J. (2016). Bridges between mitochondrial oxidative stress, ER stress and mTOR signaling in pancreatic β cells. Cell. Signal. *28*, 1099–1104. https://doi.org/10.1016/j.cellsig.2016.05.007.
3. Ardestani, A., Lupse, B., Kido, Y., Leibowitz, G., and Maedler, K. (2018). mTORC1 Signaling: A Double-Edged Sword in Diabetic β Cells. Cell Metab. *27*, 314–331. https://doi.org/10.1016/j.cmet.2017.11.004.
4. Cnop, M., Ladriere, L., Hekerman, P., Ortis, F., Cardozo, A.K., Dogusan, Z., Flamez, D., Boyce, M., Yuan, J., and Eizirik, D.L. (2007). Selective inhibition of eukaryotic translation initiation factor 2 alpha dephosphorylation potentiates fatty acid-induced endoplasmic reticulum stress and causes pancreatic beta-cell dysfunction and apoptosis. J. Biol. Chem. *282*, 3989–3997. https://doi.org/10.1074/jbc.M607627200.
5. Engin, F., Yermalovich, A., Nguyen, T., Hummasti, S., Fu, W., Eizirik, D.L., Mathis, D., and Hotamisligil, G.S. (2013). Restoration of the unfolded protein response in pancreatic β cells protects mice against type 1 diabetes. Sci. Transl. Med. *5*, 211ra156. https://doi.org/10.1126/scitranslmed.3006534.
6. González-Casimiro, C.M., Merino, B., Casanueva-Álvarez, E., Postigo-Casado, T., Cámara-Torres, P., Fernández-Díaz, C.M., Leissring, M.A., Cózar-Castellano, I., and Perdomo, G. (2021). Modulation of Insulin Sensitivity by Insulin-Degrading Enzyme. Biomedicines *9*, 86. https://doi.org/10.3390/biomedicines9010086.
7. Tundo, G.R., Sbardella, D., Ciaccio, C., Bianculli, A., Orlandi, A., Desimio, M.G., Arcuri, G., Coletta, M., and Marini, S. (2013). Insulin-degrading enzyme (IDE): a novel heat shock-like protein. J. Biol. Chem. *288*, 2281–2289. https://doi.org/10.1074/jbc.M112.393108.
8. Tundo, G.R., Sbardella, D., Ciaccio, C., Grasso, G., Gioia, M., Coletta, A., Polticelli, F., Di Pierro, D., Milardi, D., Van Endert, P., et al. (2017). Multiple functions of insulin-degrading enzyme: a metabolic crosslight? Crit. Rev. Biochem. Mol. Biol. *52*, 554–582. https://doi.org/10.1080/10409238.2017.1337707.
9. Farris, W., Mansourian, S., Chang, Y., Lindsley, L., Eckman, E.A., Frosch, M.P., Eckman, C.B., Tanzi, R.E., Selkoe, D.J., and Guenette, S. (2003). Insulin-degrading enzyme regulates the levels of insulin, amyloid beta-protein, and the beta-amyloid precursor protein intracellular domain in vivo. Proc. Natl. Acad. Sci. USA *100*, 4162–4167. https://doi.org/10.1073/pnas.0230450100.
10. Steneberg, P., Bernardo, L., Edfalk, S., Lundberg, L., Backlund, F., Ostenson, C.-G., and Edlund, H. (2013). The type 2 diabetes-associated gene ide is required for insulin secretion and suppression of α-synuclein levels in β-cells. Diabetes *62*, 2004–2014. https://doi.org/10.2337/db12-1045.
11. Villa-Pérez, P., Merino, B., Fernández-Díaz, C.M., Cidad, P., Lobatón, C.D., Moreno, A., Muturi, H.T., Ghadieh, H.E., Najjar, S.M., Leissring, M.A., et al. (2018). Liver-specific ablation of insulin-degrading enzyme causes hepatic insulin resistance and glucose intolerance, without affecting insulin clearance in mice. Metabolism *88*, 1–11. https://doi.org/10.1016/j.metabol.2018.08.001.
12. Authier, F., Metioui, M., Fabrega, S., Kouach, M., and Briand, G. (2002). Endosomal proteolysis of internalized insulin at the C-terminal region of the B chain by cathepsin D. J. Biol. Chem. *277*, 9437–9446. https://doi.org/10.1074/jbc.M110188200.
13. Duckworth, W.C., Bennett, R.G., and Hamel, F.G. (1998). Insulin acts intracellularly on proteasomes through insulin-degrading enzyme. Biochem. Biophys. Res. Commun. *244*, 390–394. https://doi.org/10.1006/bbrc.1998.8276.
14. Ralat, L.A., Kalas, V., Zheng, Z., Goldman, R.D., Sosnick, T.R., and Tang, W.-J. (2011). Ubiquitin is a novel substrate for human insulin-degrading enzyme. J. Mol. Biol. *406*, 454–466. https://doi.org/10.1016/j.jmb.2010.12.026.

15. Sbardella, D., Tundo, G.R., Coletta, A., Marcoux, J., Koufogeorgou, E.I., Ciaccio, C., Santoro, A.M., Milardi, D., Grasso, G., Cozza, P., et al. (2018). The insulin-degrading enzyme is an allosteric modulator of the 20S proteasome and a potential competitor of the 19S. Cell. Mol. Life Sci. *75*, 3441–3456. https://doi.org/10.1007/s00018-018-2807-y.
16. Llovera, R.E., de Tullio, M., Alonso, L.G., Leissring, M.A., Kaufman, S.B., Roher, A.E., de Prat Gay, G., Morelli, L., and Castaño, E.M. (2008). The catalytic domain of insulin-degrading enzyme forms a denaturant-resistant complex with amyloid beta peptide: implications for Alzheimer disease pathogenesis. J. Biol. Chem. *283*, 17039–17048. https://doi.org/10.1074/jbc.M706316200.
17. Sharma, S.K., Chorell, E., Steneberg, P., Vernersson-Lindahl, E., Edlund, H., and Wittung-Stafshede, P. (2015). Insulin-degrading enzyme prevents α-synuclein fibril formation in a nonproteolytical manner. Sci. Rep. *5*, 12531. https://doi.org/10.1038/srep12531.
18. Li, Q., Ali, M.A., and Cohen, J.I. (2006). Insulin degrading enzyme is a cellular receptor mediating varicella-zoster virus infection and cell-to-cell spread. Cell *127*, 305–316. https://doi.org/10.1016/j.cell.2006.08.046.
19. Schmitz, A., Schneider, A., Kummer, M.P., and Herzog, V. (2004). Endoplasmic reticulum-localized amyloid beta-peptide is degraded in the cytosol by two distinct degradation pathways. Traffic *5*, 89–101.
20. Beuzelin, C., Evnouchidou, I., Rigolet, P., Cauvet-Burgevin, A., Girard, P.-M., Dardalhon, D., Culina, S., Gdoura, A., van Endert, P., and Francesconi, S. (2013). Deletion of the fission yeast homologue of human insulinase reveals a TORC1-dependent pathway mediating resistance to proteotoxic stress. PLoS One *8*, e67705. https://doi.org/10.1371/journal.pone.0067705.
21. Rudovich, N., Pivovarova, O., Fisher, E., Fischer-Rosinsky, A., Spranger, J., Möhlig, M., Schulze, M.B., Boeing, H., and Pfeiffer, A.F.H. (2009). Polymorphisms within insulin-degrading enzyme (IDE) gene determine insulin metabolism and risk of type 2 diabetes. J. Mol. Med. *87*, 1145–1151. https://doi.org/10.1007/s00109-009-0540-6.
22. Fernández-Díaz, C.M., Merino, B., López-Acosta, J.F., Cidad, P., de la Fuente, M.A., Lobatón, C.D., Moreno, A., Leissring, M.A., Perdomo, G., and Cózar-Castellano, I. (2019). Pancreatic β-cell-specific deletion of insulin-degrading enzyme leads to dysregulated insulin secretion and β-cell functional immaturity. Am. J. Physiol. Endocrinol. Metab. *317*, E805–E819. https://doi.org/10.1152/ajpendo.00040.2019.
23. Maianti, J.P., McFedries, A., Foda, Z.H., Kleiner, R.E., Du, X.Q., Leissring, M.A., Tang, W.-J., Charron, M.J., Seeliger, M.A., Saghatelian, A., and Liu, D.R. (2014). Anti-diabetic activity of insulin-degrading enzyme inhibitors mediated by multiple hormones. Nature *511*, 94–98. https://doi.org/10.1038/nature13297.
24. Deprez-Poulain, R., Hennuyer, N., Bosc, D., Liang, W.G., Enée, E., Marechal, X., Charton, J., Totobenazara, J., Berte, G., Jahklal, J., et al. (2015). Catalytic site inhibition of insulin-degrading enzyme by a small molecule induces glucose intolerance in mice. Nat. Commun. *6*, 8250. https://doi.org/10.1038/ncomms9250.
25. Guo, Q., Manolopoulou, M., Bian, Y., Schilling, A.B., and Tang, W.-J. (2010). Molecular basis for the recognition and cleavages of IGF-II, TGF-alpha, and amylin by human insulin-degrading enzyme. J. Mol. Biol. *395*, 430–443. https://doi.org/10.1016/j.jmb.2009.10.072.
26. Shen, Y., Joachimiak, A., Rosner, M.R., and Tang, W.-J. (2006). Structures of human insulin-degrading enzyme reveal a new substrate recognition mechanism. Nature *443*, 870–874. https://doi.org/10.1038/nature05143.
27. Sachdeva, M.M., Claiborn, K.C., Khoo, C., Yang, J., Groff, D.N., Mirmira, R.G., and Stoffers, D.A. (2009). Pdx1 (MODY4) regulates pancreatic beta cell susceptibility to ER stress. Proc. Natl. Acad. Sci. USA *106*, 19090–19095. https://doi.org/10.1073/pnas.0904849106.
28. Jones, H.B., Nugent, D., and Jenkins, R. (2010). Variation in characteristics of islets of Langerhans in insulin-resistant, diabetic and non-diabetic-rat strains. Int. J. Exp. Pathol. *91*, 288–301. https://doi.org/10.1111/j.1365-2613.2010.00713.x.
29. Chen, W.-P., Chi, T.-C., Chuang, L.-M., and Su, M.-J. (2007). Resveratrol enhances insulin secretion by blocking K(ATP) and K(V) channels of beta cells. Eur. J. Pharmacol. *568*, 269–277. https://doi.org/10.1016/j.ejphar.2007.04.062.
30. Lee, J.-H., and Lee, J. (2022). Endoplasmic Reticulum (ER) Stress and Its Role in Pancreatic β-Cell Dysfunction and Senescence in Type 2 Diabetes. Int. J. Mol. Sci. *23*, 4843. https://doi.org/10.3390/ijms23094843.
31. Scheuner, D., and Kaufman, R.J. (2008). The unfolded protein response: a pathway that links insulin demand with beta-cell failure and diabetes. Endocr. Rev. *29*, 317–333. https://doi.org/10.1210/er.2007-0039.
32. Wu, J., Rutkowski, D.T., Dubois, M., Swathirajan, J., Saunders, T., Wang, J., Song, B., Yau, G.D.-Y., and Kaufman, R.J. (2007). ATF6alpha optimizes long-term endoplasmic reticulum function to protect cells from chronic stress. Dev. Cell *13*, 351–364. https://doi.org/10.1016/j.devcel.2007.07.005.
33. Preissler, S., and Ron, D. (2019). Early events in the endoplasmic reticulum unfolded protein response. Cold Spring Harb. Perspect. Biol. *11*, a033894. https://doi.org/10.1101/cshperspect.a033894.
34. Akiyama, T., Takasawa, S., Nata, K., Kobayashi, S., Abe, M., Shervani, N.J., Ikeda, T., Nakagawa, K., Unno, M., Matsuno, S., and Okamoto, H. (2001). Activation of Reg gene, a gene for insulin-producing beta -cell regeneration: poly(ADP-ribose) polymerase binds Reg promoter and regulates the transcription by autopoly(ADP-ribosyl)ation. Proc. Natl. Acad. Sci. USA *98*, 48–53. https://doi.org/10.1073/pnas.240458597.
35. Unno, M., Nata, K., Noguchi, N., Narushima, Y., Akiyama, T., Ikeda, T., Nakagawa, K., Takasawa, S., and Okamoto, H. (2002). Production and characterization of Reg knockout mice: reduced proliferation of pancreatic beta-cells in Reg knockout mice. Diabetes *51*, S478–S483.
36. Watanabe, T., Yonemura, Y., Yonekura, H., Suzuki, Y., Miyashita, H., Sugiyuma, K., Moriizumi, S., Unno, M., Tanaka, O., Kondo, H., et al. (1993). Pancreatic beta-cell replication and amelioration of surgical diabetes by Reg protein. Pros. Natl. Acad. Sci. USA *91*, 3589–3592.
37. Gross, D.J., Weiss, L., Reibstein, I., van den Brand, J., Okamoto, H., Clark, A., and Slavin, S. (1998). Amelioration of diabetes in nonobese diabetic mice with advanced disease by linomide-induced immunoregulation combined with Reg protein treatment. Endocrinology *139*, 2369–2374. https://doi.org/10.1210/endo.139.5.5997.
38. Liu, L., Chowdhury, S., Fang, X., Liu, J.-L., and Srikant, C.B. (2014). Attenuation of unfolded protein response and apoptosis by mReg2 induced GRP78 in mouse insulinoma cells. FEBS Lett. *588*, 2016–2024. https://doi.org/10.1016/j.febslet.2014.04.030.
39. Jarchum, I., Takaki, T., and DiLorenzo, T.P. (2008). Efficient culture of CD8(+) T cells from the islets of NOD mice and their use for the study of autoreactive specificities. J. Immunol. Methods *339*, 66–73. https://doi.org/10.1016/j.jim.2008.08.007.
40. Sobota, J.A., Bäck, N., Eipper, B.A., and Mains, R.E. (2009). Inhibitors of the V0 subunit of the vacuolar H+-ATPase prevent segregation of lysosomal- and secretory-pathway proteins. J. Cell Sci. *122*, 3542–3553. https://doi.org/10.1242/jcs.034298.
41. Rahimi, R., Malek, I., Lerrer-Goldshtein, T., Elkis, Y., Shoval, I., Jacob, A., Shpungin, S., and Nir, U. (2021). TMF1 is upregulated by insulin and is required for a sustained glucose homeostasis. FASEB J. *35*, e21295. https://doi.org/10.1096/fj.202001995R.
42. Ravassard, P., Hazhouz, Y., Pechberty, S., Bricout-Neveu, E., Armanet, M., Czernichow, P., and Scharfmann, R. (2011). A genetically engineered human pancreatic β cell line exhibiting glucose-inducible insulin secretion. J. Clin. Invest. *121*, 3589–3597. https://doi.org/10.1172/JCI58447.
43. Donath, M.Y., and Shoelson, S.E. (2011). Type 2 diabetes as an inflammatory disease. Nat. Rev. Immunol. *11*, 98–107. https://doi.org/10.1038/nri2925.
44. Cambiaghi, T.D., Pereira, C.M., Shanmugam, R., Bolech, M., Wek, R.C., Sattlegger, E., and Castilho, B.A. (2014). Evolutionarily conserved IMPACT impairs various stress responses that require GCN1 for activating the eIF2 kinase GCN2. Biochem. Biophys. Res. Commun. *443*, 592–597. https://doi.org/10.1016/j.bbrc.2013.12.021.
45. You, K., Wang, L., Chou, C.-H., Liu, K., Nakata, T., Jaiswal, A., Yao, J., Lefkovith, A., Omar, A., Perrigoue, J.G., et al. (2021). QRICH1 dictates the outcome of ER stress through transcriptional control of proteostasis. Science *371*, eabb6896. https://doi.org/10.1126/science.abb6896.
46. Carpenter, J.E., Jackson, W., de Souza, G.A., Haarr, L., and Grose, C. (2010). Insulin-degrading enzyme binds to the nonglycosylated precursor of varicella-zoster virus gE protein found in the endoplasmic reticulum. J. Virol. *84*, 847–855. https://doi.org/10.1128/JVI.01801-09.
47. Davidson, S., Yu, C.-H., Steiner, A., Ebstein, F., Baker, P.J., Jarur-Chamy, V., Hrovat Schaale, K., Laohamonthonkul, P., Kong, K., Calleja, D.J., et al. (2022). Protein kinase R is an innate immune sensor of proteotoxic stress via accumulation of cytoplasmic IL-24. Sci. Immunol. *7*, eabi6763. https://doi.org/10.1126/sciimmunol.abi6763.
48. Costa-Mattioli, M., and Walter, P. (2020). The integrated stress response: From mechanism to disease. Science *368*, eaat5314. https://doi.org/10.1126/science.aat5314.

49. Ying, W., Lee, Y.S., Dong, Y., Seidman, J.S., Yang, M., Isaac, R., Seo, J.B., Yang, B.-H., Wollam, J., Riopel, M., et al. (2019). Expansion of Islet-Resident Macrophages Leads to Inflammation Affecting β Cell Proliferation and Function in Obesity. Cell Metab. *29*, 457–474.e5. https://doi.org/10.1016/j.cmet.2018.12.003.
50. Kahn, S.E., Hull, R.L., and Utzschneider, K.M. (2006). Mechanisms linking obesity to insulin resistance and type 2 diabetes. Nature *444*, 840–846. https://doi.org/10.1038/nature05482.
51. Sharma, R.B., O'Donnell, A.C., Stamateris, R.E., Ha, B., McCloskey, K.M., Reynolds, P.R., Arvan, P., and Alonso, L.C. (2015). Insulin demand regulates β cell number via the unfolded protein response. J. Clin. Invest. *125*, 3831–3846. https://doi.org/10.1172/JCI79264.
52. Teodoro, T., Odisho, T., Sidorova, E., and Volchuk, A. (2012). Pancreatic β-cells depend on basal expression of active ATF6α-p50 for cell survival even under nonstress conditions. Am. J. Physiol. Cell Physiol. *302*, C992–C1003. https://doi.org/10.1152/ajpcell.00160.2011.
53. Merino, B., Casanueva-Álvarez, E., Quesada, I., González-Casimiro, C.M., Fernández-Díaz, C.M., Postigo-Casado, T., Leissring, M.A., Kaestner, K.H., Perdomo, G., and Cózar-Castellano, I. (2022). Insulin-degrading enzyme ablation in mouse pancreatic alpha cells triggers cell proliferation, hyperplasia and glucagon secretion dysregulation. Diabetologia *65*, 1375–1389. https://doi.org/10.1007/s00125-022-05729-y.
54. Liu, M., Wang, Z., Ren, M., Yang, X., Liu, B., Qi, H., Yu, M., Song, S., Chen, S., Liu, L., et al. (2019). SIRT4 regulates PTEN stability through IDE in response to cellular stresses. FASEB J. *33*, 5535–5547. https://doi.org/10.1096/fj.201801987R.
55. Park, Y., Reyna-Neyra, A., Philippe, L., and Thoreen, C.C. (2017). mTORC1 Balances Cellular Amino Acid Supply with Demand for Protein Synthesis through Post-transcriptional Control of ATF4. Cell Rep. *19*, 1083–1090. https://doi.org/10.1016/j.celrep.2017.04.042.
56. Binger, K.J., Neukam, M., Tattikota, S.G., Qadri, F., Puchkov, D., Willmes, D.M., Wurmsee, S., Geisberger, S., Dechend, R., Raile, K., et al. (2019). Atp6ap2 deletion causes extensive vacuolation that consumes the insulin content of pancreatic β cells. Proc. Natl. Acad. Sci. USA *116*, 19983–19988. https://doi.org/10.1073/pnas.1903678116.
57. Nakayama, M., Abiru, N., Moriyama, H., Babaya, N., Liu, E., Miao, D., Yu, L., Wegmann, D.R., Hutton, J.C., Elliott, J.F., and Eisenbarth, G.S. (2005). Prime role for an insulin epitope in the development of type 1 diabetes in NOD mice. Nature *435*, 220–223. https://doi.org/10.1038/nature03523.
58. Nash, Y., Ganoth, A., Borenstein-Auerbach, N., Levy-Barazany, H., Goldsmith, G., Kopelevich, A., Pozyuchenko, K., Sakhneny, L., Lazdon, E., Blanga-Kanfi, S., et al. (2021). From virus to diabetes therapy: Characterization of a specific insulin-degrading enzyme inhibitor for diabetes treatment. FASEB J. *35*, e21374. https://doi.org/10.1096/fj.201901945R.
59. Serreze, D.V., Chapman, H.D., Varnum, D.S., Hanson, M.S., Reifsnyder, P.C., Richard, S.D., Fleming, S.A., Leiter, E.H., and Shultz, L.D. (1996). B lymphocytes are essential for the initiation of T cell-mediated autoimmune diabetes: analysis of a new "speed congenic" stock of NOD.Ig mu null mice. J. Exp. Med. *184*, 2049–2053. https://doi.org/10.1084/jem.184.5.2049.
60. Arreaza, G.A., Cameron, M.J., Jaramillo, A., Gill, B.M., Hardy, D., Laupland, K.B., Rapoport, M.J., Zucker, P., Chakrabarti, S., Chensue, S.W., et al. (1997). Neonatal activation of CD28 signaling overcomes T cell anergy and prevents autoimmune diabetes by an IL-4-dependent mechanism. J. Clin. Invest. *100*, 2243–2253. https://doi.org/10.1172/JCI119762.
61. Oshima, M., Knoch, K.-P., Diedisheim, M., Petzold, A., Cattan, P., Bugliani, M., Marchetti, P., Choudhary, P., Huang, G.-C., Bornstein, S.R., et al. (2018). Virus-like infection induces human β cell dedifferentiation. JCI Insight *3*, e97732. https://doi.org/10.1172/jci.insight.97732.

STAR★METHODS

KEY RESOURCES TABLE

REAGENT or RESOURCE	SOURCE	IDENTIFIER
Antibodies		
Rabbit monoclonal anti-phosphor-PERK	Cell signaling	Cat# 3179; RRID: AB_2095853
Rabbit monoclonal anti-PERK	Cell signaling	Cat# 3192; RRID: AB_2095847
Rabbit polyclonal anti-phosphor-eIF2α	Cell signaling	Cat# 9721; RRID: AB_330951
Rabbit polyclonal anti-eIF2α	Cell signaling	Cat# 9722; RRID: AB_2230924
Mouse monoclonal anti-ATF6	Novus Biologicals	Cat# NBP1-40256; RRID: AB_2058774
Rabbit monoclonal anti-PCNA	Abcam	Cat# ab92552; RRID: AB_10561973
Mouse monoclonal anti-β-actin	Santa Cruz	Cat# sc-47778; RRID: AB_2714189
Alexa Fluor® 647 Mouse anti-Ki-67	BD Biosciences	Cat# BD558615; RRID: AB_647130
Guinea pig polyclonal anti-insulin	Abcam	Cat# ab7842; RRID: AB_306130
Mouse monoclonal anti-IDE	Santa Cruz	Cat# sc-393887; RRID: AB_2800507
Goat polyclonal anti-IDE	Santa Cruz	Cat# sc-27266
Horseradish peroxidase-labelled anti-rabbit IgG	Cell signaling	Cat# 7074; RRID: AB_2099233
Horseradish peroxidase-labelled anti-mouse IgG	Cell signaling	Cat# 7076; RRID: AB_330924
Goat anti-guinea pig Alexa Fluor 594	nvitrogen	Cat# A-11076; RRID: AB_141930
Goat anti-guinea pig Alexa Fluor 488	Invitrogen	Cat# A-11073; RRID: AB_2534117
Chemicals, peptides, and recombinant proteins		
Collagenase P	Roche	Cat# 11213865001
Tunicamycin	Tunicamycin	Cat# T7765
Rapamycin	LC laboratories	Cat# R-5000
Salubrinal	Sigma-Aldrich	Cat# SML0951
Epoxomicin	Sigma-Aldrich	Cat# 134381-21-8
Thapsigargin	Sigma-Aldrich	Cat# T9033
Carfilzomib	Tocris	Cat# 7188
Recombinant REG2	R&D Systems	Cat# 2098-RG
Human insulin	Roche	Cat# 11376497
RLT lysis buffer	Qiagen	Cat# 1015750
RIPA lysis buffer	Thermo scientific	Cat# 89900
EDTA-free Protease inhibitor cOmplete	Roche	Cat# 11836170001
PhosSTOP phosphatase inhibitor cocktails	Roche	Cat# 4906845001
4x LDS NuPAGE sample buffer	Invitrogen	Cat# NP0007
10x sample reducing agent	Invitrogen	Cat# NP0004
4-12% NuPAGE Bis-Tris gels	Invitrogen	Cat# NP0321BOX
SYPRO® Ruby Protein Gel Stain	Molecular Probes	Cat# S12000
SuperSignal West Femto maximum sensitivity substrate	Thermo scientific	Cat# PI34095
West Pico plus chemiluminescent substrate	Thermo scientific	Cat# 34580
Antigenfix	Diapath	Cat# P0014

(*Continued on next page*)

Continued

REAGENT or RESOURCE	SOURCE	IDENTIFIER
Universal HIER antigen retrieval reagent	Abcam	Cat# 208572
Vectashield mounting media	Vector Laboratories Inc	Cat# NC9532821
Blocking buffer	Cell signaling	Cat# 12411S
DAPI	Thermo scientific	Cat# D1306, RRID: AB_2629482
Critical commercial assays		
NucleoSpin RNA XS kit	Macherey-Nagel	Cat# 740902.50
High-capacity cDNA reverse transcription kit	Applied Biosystems	Cat# 43-688-14
Power SYBR Green PCR Master mix	Applied Biosystems	Cat# 4367659
Click-iT™ EdU imaging kit	Invitrogen	Cat#C10337
NanoRSLC-Q Exactive Plus Mass Spectrometer	Thermo Scientific	Dionex Ultimate 3000, RRID: SCR_020563
Mouse insulin ELISA kit	Mercodia	Cat# 10-1247-01, RRID: AB_2783837
Mouse proinsulin ELISA kit	Mercodia	Cat# 10-1232-01
Mouse IAPP ELISA kit	Bachem	Cat# 124447-81-0
Deposited data		
Raw proteomics data (Figure 2J)	This paper	PRIDE (EMBL-EBI): PXD034826
Raw RNA-sequencing data (Figure 7, S8)	This paper	GEO: GSE207797
Experimental models: Cell lines		
Human EndoC-βH1 cell line	Human cell design	J Clin Invest. 2011; 121(9):3589-3597
Experimental models: Organisms/strains		
NOD/ShiLtJ	Internal breeding	JAX: #0011976. RRID: IMSR_JAX:001976
NOD/ShiLtJ-*Ide*$^{-/-}$	Internal breeding	This paper
C57BL/6J	Internal breeding	JAX: #000664.RRID: IMSR_JAX:000664
C57BL/6J-*Ide*$^{-/-}$	Internal breeding	Proc Natl Acad Sci U S A. 2003 Apr 1; 100(7): 4162–4167.
Oligonucleotides		
	See Table S3 for list of oligonucleotides	
Software and algorithms		
ImageJ	NIH	https://imagej.nih.gov/ij/
Prism 10	Graphpad	https://www.graphpad.com/scientific-software/prism/
Icy	on GitHub	https://icy.bioimageanalysis.org/
QuPath versio 0.5.0	on GitHub	https://github.com/qupath/qupath/releases/tag/v0.5.0
MaxQuant version 1.6.17	Cox and Mann	RRID: SCR_014485
UniProtKB/Swiss-Prot		RRID: SCR_021164
Perseus software version 1.6.14		RRID: SCR_015753
Enrichr		RRID: SCR_001575
Python		RRID: SCR_008394
Other		
Accu-Check glucometer	Roche	
I-Blot2	Invitrogen	Cat# IB21001
JEOL 1011 transmission electron microscope		
Leica SP8 confocal microscope	Leica	
Leica SP8 SMD confocal microscope		

RESOURCE AVAILABILITY

Lead contact

Further information and requests for resources and reagents should be directed to and will be fulfilled by the lead contact, Peter van Endert (vanendert@me.com).

Materials availability

This study did not generate new unique reagents.

Data and code availability

The mass spectrometry proteomics data have been deposited to the ProteomeXchange Consortium via the PRIDE partner repository with the dataset identifier PXD034826 and 10.6019/PXD034826. The GEO accession number for RNAseq datasets is GSE207797. All source data and mouse lines included in this study are available from the corresponding author upon reasonable request. This paper does not report original code.

EXPERIMENTAL MODEL AND STUDY PARTICIPANT DETAILS

Animals

Ide$^{-/-}$ mice on a C57BL/6 background were obtained from S. Guenette.[9] NOD.*ide* congenic stock was generated using a marker-assisted breeding approach to speed up the introgression of the *Ide*-disrupted gene from the C57BL/6 congenic mice onto a NOD genetic background.[59] Specifically, a panel of 36 informative microsatellite markers was chosen to cover all the insulin-dependent diabetes (Idd) susceptibility loci of the NOD mice known at the time (I*dd1* to *Idd20*). Although microsatellites analyses confirmed that all NOD *Idd* loci had been fixed after 5 generations, another 5 back-crosses to NOD mice were performed. The presence of the desired *Ide*$^{+/+}$ or *Ide*$^{-/-}$ genotypes was routinely verified by PCR using the primers, WT Forward: 5′-ATCTG TGTCA GGAGG AGGGA C, WT Reverse: 5′-CAGGG TAGGG AAGTC AAGGT TAC, and NEO Forward: 5′-GGGCG CCCGG TTCTT TDTTTGT C, NEO Reverse: 5′: TTGGT GGTCG AATGG GCAGG T. C57BL/6J, C57BL/6J *Ide*$^{-/-}$, and NOD *Ide*$^{+/+}$, NOD *Ide*$^{-/-}$, and NOD *Ide*$^{-/-}$ *Rag2*$^{-/-}$ were bred and housed in an ambient temperature room with 12/12 h light/dark cycles and specific pathogen-free conditions. Both female and male wt and *Ide*$^{-/-}$ C57BL/6 and NOD mice aged up to 30 weeks were studied in the different experiments. In wt mice with the genetic NOD background, females develop spontaneous autoimmune diabetes at a much higher rate (about 80%) than males (about 20%). Ethical approval for animal experimentation in this project was accorded by the Ministère de l'enseignement, de la recherche et de l'innovation on October 8, 2020, for a duration of 5 years under the number APAFIS#27441-2019080809515121.

METHOD DETAILS

Insulitis scoring

Pancreata were fixed in 4% formalin for at least 2 h, embedded in paraffin overnight and mounted in a paraffin block. Four μm paraffin sections were mounted onto Superfrost™ slides coated with albumin, dried, deparaffinized and re-hydrated in 100%, 90%, 80% alcohol baths. Sections were stained in hematoxylin and eosin, each for 2 min, and mounted with EUKIT and a coverslip. For each pancreas, 30 islets were scored for insulitis using the following classification[60]: 0: normal, 1: peri-insulitis, 2: moderate insulitis (less than 50% of mononuclear cells) 3: severe insulitis (more than 50% of mononuclear cells and/or loss of islet architecture).

Spontaneous diabetes incidence

The onset of diabetes was defined as two positive urine glucose tests, confirmed by a glycemia >200 mg/dL. Glucose tests and measure of glycemia were performed in a blind fashion.

Oral glucose tolerance test (OGTT)

OGTT experiments were performed on female *Ide*$^{+/+}$ and *Ide*$^{-/-}$ NOD mice as described in ref. [24]. Following a 6 h fasting period, basal blood glucose was determined and a bolus of glucose at 2 g/kg was administered by gavage. Blood glucose levels were determined using an Accu-Check glucometer (Roche). Plasma concentrations were measured by ELISA kit (Mercodia) in blood samples collected 15 min before and 15, 90 and 180 min after glucose administration.

Estimation of islet volume

Islets from 15 female C57BL/6 or NOD mice aged 8 weeks per group were stained for insulin using polyclonal guinea pig antibody against mouse insulin (Abcam) to outline the islet surface and imaged by fluorescence microscopy. An average of 40 planes per islet were acquired. The evolution of C57BL/6 islet volume over time was evaluated by imaging islets from mice aged 6, 10 and 14 weeks in the same manner. Islet volume was determined using Icy software and the plug-in ROI Statistics developed by members of the Biological Image Analysis unit of the Institute Pasteur, Paris.

Pancreatic islet preparation

Mice were sacrificed, the peritoneal cavity was opened. Ice-cold collagenase P (Roche; 0.76 mg/ml in HBSS) was injected through a catheter introduced into the part of the bile duct running from the liver to the pancreas (2 ml/mouse). The instilled pancreas was extracted and digested for 10 min at 37°C, digestion was stopped by addition of cold HBSS with 10% FCS. The islets were handpicked under the microscope.

IAPP quantification in serum

To determine IAPP levels in blood, undiluted serum from female mice of different age was analyzed using a commercial ELISA kit (Bachem).

Glucose-stimulated insulin secretion (GSIS)

15 similarly sized islets were preincubated in fresh DMEM with 10% FCS without glucose for 90 min, followed by 1 h of incubation in DMEM with 2.8- or 28-mM glucose. Insulin content in supernatants was quantified using an insulin ELISA (Mercodia).

RNA preparation and qPCR analysis

Total RNA of isolated islets was extracted using NucleoSpin RNA XS kit (Macherey-Nagel), then normalized RNA was transformed into cDNA using the High-capacity cDNA reverse transcription kit (Applied Biosystems). QPCR was performed on a 7900HT fast real-time PCR system (Applied Biosystems) to identify gene expression. Relative gene expression levels were expressed as ΔΔCt (fold change), and the primers used are listed in the key resources table.

Digestions with recombinant IDE

Recombinant mouse REG2 (R&D Systems) and human insulin (Roche) were digested with recombinant WT or protease-dead (cf-E111Q) human IDE enzyme[25] in 20 mM Hepes pH 7.2, 50 mM NaCl buffer at a ratio IDE : INS ratio (w/w) of 1:1, or a ratio IDE : REG2 of 1:10. Enzymes and substrates were incubated with end-over-end rotation at 37°C for 5 s to 5 min for insulin, and for 30 min to 8 h for REG2. Samples were resolved by 4-12% NuPAGE Bis-Tris gels (Invitrogen), stained with SYPRO® Ruby Protein Gel Stain (Molecular Probes) and visualized using a UV source.

Electron microscopy

Islets from 3 female 10-week-old *Ide*$^{+/+}$ and 3 *Ide*$^{-/-}$ mice were prepared and immersion fixed in 4% paraformaldehyde (PFA) and 2.5% glutaraldehyde in 0.1M sodium phosphate pH 7.2 for at least 2 hours and stored at 4°C in 4% PFA until further processing. Islet samples were dehydrated, embedded in epoxy resin, and processed to ultra-thin 90 nm sections using Reichert Ultracut S equipment and diatome blades. Images were acquired on a JEOL 1011 transmission electron microscope. Images were evaluated for beta cell area, dense core area, granule halo area and number of secretory granules per cell using QuPath software (version 0.5.0).

Proteomic analysis of NOD islets

Samples from 3 *Ide*$^{+/+}$ and 3 *Ide*$^{-/-}$ female mice aged 10 weeks (~100 islets per sample) were prepared, digested with trypsin and then resuspended in 10% ACN, 0.1% TFA in HPLC-grade water. Each sample was injected three times in a nanoRSLC-Q Exactive PLUS (RSLC Ultimate 3000) (Thermo Scientific). Peptides were loaded onto a μ-precolumn (Acclaim PepMap 100 C18, cartridge, 300 μm i.d.×5 mm, 5 μm) (Thermo Scientific), and separated on a 50 cm reversed-phase liquid chromatographic column (0.075 mm ID, Acclaim PepMap 100, C18, 2 μm) (Thermo Scientific). Peptides were eluted and analyzed by data dependent MS/MS, using top-10 acquisition method. Peptides were fragmented using higher-energy collisional dissociation (HCD). The MS files were processed with the MaxQuant software version 1.6.17 and searched with the Andromeda search engine against the UniProtKB/Swiss-Prot Mus Musculus database (release of February 2021, 17071 entries). Proteins were quantified according to the MaxQuant label-free algorithm using LFQ intensities. Statistical and bioinformatic analysis were performed with Perseus software (version 1.6.14) (www.perseus-framework.org). We performed a two-sample t-test with a p-value threshold of 0.05. The differentially expressed proteins were subjected to bioinformatics analysis using EnrichR software (https://maayanlab.cloud/Enrichr/) for enrichment of GO terms using GO Biological Process library from 2021 (Table S2). TOP10 enriched terms were ranked using adjusted p-value ranking. Volcano-plot and enrichment bar-plot were made using Python (version 3.8.3).

ER stress

Mice either received an intraperitoneal injection of PBS (10 mL/kg, control group) or tunicamycin (Sigma-Aldrich; 2 mg/kg) or two injections of rapamycin (LC laboratories; 5 mg/kg at day1 and day 2) or tunicamycin + rapamycin, or tunicamycin + salubrinal (Sigma-Aldrich; 1.5 mg/kg). Mice were sacrificed 24 h to 48 h post-injection.

EndoC-βH1 experiments

The Human EndoC-βH1 cell line[42] was cultured in Advanced/DMEMF12 media supplemented with BSA, nicotinamide, β-Mercaptoethanol, sodium selenite, glutamax, and antibiotics. To ensure the absence of mycoplasma contamination, cells were screened prior to experimentation.

Cells were transfected as described[61] using lipofectamine RNAiMax with either 80 nM of scramble control siRNA or IDE targeting siRNA (Horizon Discovery). Following a 72-hour incubation period post-transfection, cells were treated with epoxomicin (1 μM), tunicamycin (10 μM), rapamycin (50 nM), or thapsigargin (500 nM) for 18 hours. After treatment, cells were washed with PBS and lysed with RLT lysis buffer before mRNA extraction (Qiagen). SYBR green-based RT-qPCR was performed using QuantStudio3. Primers used are described in the STAR Methods key resources table. The housekeeping gene *PPIA* was used as an internal control for normalization purposes.

Primary human islet test

Islets from a cadaveric donor (male, BMI 32.4, age 48) were purchased from Tebu-Bio (Le Perray en Yvelines, France) and cultured in PIM(S) medium supplemented with PIM(G), PIM(ABS) and Penicillin/Streptomycin. Dispersed islets were treated with IDE inhibitor BDM 44768 for 24 h before extraction of RNA that was transcribed to cDNA using the High Capacity cDNA reverse transcription kit (Applied Biosystems). Quantitative PCR reactions were run on a 7900HT real-time PCR system (Applied Biosystems).

Immunoblots

Isolated islets were homogenized in RIPA lysis buffer (Thermo scientific) containing protease (Roche) and phosphatase inhibitor cocktails (Roche). Samples were resolved by 4-12% NuPAGE Bis-Tris gels (Invitrogen), electrotransferred to polyvinylidene difluoride membranes using I-Blot2 (Invitrogen), and probed overnight at 4°C with primary antibodies against phospho-PERK, total PERK, phospho-eIF2α, total eIF2α, ATF6, PCNA and β-actin. Detection was performed using HRP-labelled anti-rabbit/mouse IgG and developed with SuperSignal West Femto maximum sensitivity substrate (Thermo scientific) or West Pico plus chemiluminescent substrate (Thermo scientific), then quantified using ImageJ Software. Antibodies are listed in the key resources table.

HFD treatment and follow up

Seven-week-old female *Ide*$^{+/+}$ and *Ide*$^{-/-}$ C57BL/6J mice were fed a standard chow (VRF1, Special Diets Services) or HFD (D12492, Brogaarden) for 7 weeks (Figures 5 and 6 all panels except Figure 6F); or for 8 weeks (Figure 6F). Body weight was recorded once a week, and non-fasting glucose concentrations were monitored weekly using Accu-Check glucometer (Roche). Plasma and islet insulin and proinsulin concentrations were measured by commercial ELISA kits (Mercodia). For RNAseq analysis of handpicked islets, mice were fed a HFD for 2 weeks.

Immunocytology

Handpicked islets were seeded on SuperFrost Gold Plus microscope slides. For Ki67 staining, islets were fixed with 4% PFA, permeabilized with 0.1% Triton and stained with anti-Ki67, insulin antibody was used to identify islet contours. Nuclei were stained with DAPI (Thermo Fisher Scientific). Image acquisition was performed using a Leica SP8 confocal microscope. Ki67 positive cells and islet volumes were estimated with Icy Software. To assess specifically Ki67 expression by beta cells in islets from mice subjected to HFD (Figure 6F), 15 islets per group were analyzed in stacks of 20 planes. For each plane, the proximity co-efficient between Ki67 and insulin staining was calculated using Icy software. In brief, a binary mask of fluorescence signal positive for Ki67 or insulin was created by applying a fixed fluorescence threshold specific for each protein to all stack images. Two binary masks were created to create a new binary overlay mask, in which positive signal indicates a close proximity between Ki67 and insulin. The proximity coefficient of Ki67 with insulin protein was then calculated as the proportion of the positive signal in the overlay mask that overlays the signal in the insulin binary mask.

EdU staining

EdU was intraperitoneal injected (100 μg/g) into mice. The pancreas was harvested 1 h later, fixed in Antigenfix (Diapath) and embedded in paraffin blocks. Sections (5-μm-thick) were cut, deparaffinized in xylene, rehydrated followed by antigen retrieval (Abcam). EdU staining was conducted using the Click-iT™ EdU imaging kit (Invitrogen) according to the manufacturer's protocol. Anti-insulin was used to identify β-cells. Slides were mounted with Vectashield mounting media (Vector Laboratories Inc). For each mouse eight randomly selected sections were included for analysis. Images were captured using a Leica SP8 SMD confocal microscope and EdU-positive β-cells were counted.

RNAseq analysis

Total RNA samples were sent for library preparation and sequencing on an Illumina Nextseq 500 instrument. A primary analysis based on AOZAN software (ENS, Paris) was applied to demultiplex and control the quality of the raw data (based of FastQC modules/version 0.11.5). Fastq files were aligned using STAR algorithm (version 2.7.6a), on the Ensembl Mus musculus GRCm38 reference, release 101. Reads were then counted using RSEM (v1.3.1) and the statistical analyses on the read counts were performed with R (version 3.6.3) and the DESeq2 package (version 1.26.0) to determine the proportion of differentially expressed genes (DEGs) between two conditions. Cluster analysis was performed by hierarchical clustering using the Spearman correlation similarity measure and ward linkage algorithm. Heatmaps were made with the ggplot2 (version 3.3.5) and NMF (version 0.23.0) packages and a custom color palette from the RColorBrewer package (version 1.1-2). DEGs with a minimal overlap of 3, a P-value cutoff of 0.01 and a minimal enrichment of 1.5 were selected for the Pathway & Process Enrichment analysis. Input genes lists were included: GO Molecular Functions; GO Biological Processes, Reactome Gene Sets, KEGG Pathway; GO Cellular Components. The output lists of terms were then filtered to select pathways with adjusted p-values (q-values) <0.01. The criteria to select pathways to be plotted are described in figure labels.

QUANTIFICATION AND STATISTICAL ANALYSIS

Statistical analyses were carried out using GraphPad Prism Version 10. Statistical differences were evaluated using two-tailed unpaired Student t test for comparisons of one variable between two groups, one-way ANOVA and appropriate post hoc analyses for comparisons of one parameter between multiple groups and two-way ANOVA with post hoc statistical adjustment for comparisons of two or more parameters between multiple groups; Tukey's, Dunn's, Dunnett's or Sidak's correction were applied for multiple comparisons as indicated in the figure legends. A p value of less than 0.05 (*$P < 0.05$, **$P < 0.01$, and ***$P < 0.001$) was considered statistically significant. No statistical method was used to predetermine sample size. p values of multiple comparisons were always corrected using appropriate methods, as indicated. The experiments were not randomized and the investigators were not blinded to allocation during experiments and outcome assessment (except for the test of spontaneous diabetes incidence). No animal was excluded from analysis.